Fabrication of ZSM-5 and its ion exchange for naphtha cracking

By

Rabeeah Taj

School of Chemical and Materials Engineering (SCME)
National University of Sciences and Technology (NUST)
2019

Fabrication of ZSM-5 and its ion exchange for naphtha cracking

Name: Rabeeah Taj

Reg. No: 00000172153

This work is submitted as a MS thesis in partial fulfillment of the requirement for the degree of

MS in Chemical Engineering

Supervisor Name: Dr. Arshad Hussain

Co-Supervisor: Dr. Erum Pervaiz

School of Chemical and Materials Engineering (SCME)

National University of Sciences and Technology (NUST)

H-12 Islamabad Pakistan

December 2019

Dedication

To my family and friends

Acknowledgements

Praise is due to **Allah** whose worth cannot be described by speakers, whose bounties cannot be counted by calculators, whom the height of intellectual courage cannot appreciate, and the diving's of understanding cannot reach; He for whose description no limit has been laid down, no eulogy exists, no time is ordained, and no duration is fixed.

I would like to acknowledge and express my sincere gratitude my research supervisor, **Dr. Arshad Hussain** for his endless support, supervision and affectionate guidance to steer me in the right the direction whenever he thought I needed it. I would also like to extend my gratitude to committee members; **Dr. Erum Pervaiz** (co-supervisor), **Dr. Sarah Farrukh** and **Dr. Habib Nasir** for their valuable suggestions and guidance.

I would also like to thank **Dr. Saram** (NESCOM)for providing me opportunity to perform my naphtha cracking reactions through a research-oriented platform and helped me accomplishing this research work.

In the end, I must express my very profound gratitude to my parents for providing me with unfailing support and continuous encouragement throughout my years of study and through the process of researching and writing this thesis. This accomplishment would not have been possible without them.

Rabeeah Taj

Abstract

Light olefins are the backbone of modern industrialization. For more than a half century, steam/thermal hydrocarbon cracking is considered as the main route and conventional process for light olefins yield. Few drawbacks of conventional steam cracking such as extensive energy consumption, high temperature requirement and excess emission of CO_2 relate to this technology, which cannot accommodate further needs regarding the chemical process industry. Catalytic cracking of hydrocarbons is a less energy consuming and an environmentally-friendly process for light olefins production. Nowadays petroleum-extracted naphtha catalytic cracking is mainly used process. In this study, ZSM-5 is synthesized via hydrothermal crystallization method using structural directing agents (TPABr and TPAOH). The physiochemical characteristics of calcined and ion-exchanged ZSM-5 samples are well characterized by X-ray diffraction (XRD), scanning electron microscopy (SEM), Fourier transform infrared spectroscopy (FTIR), differential thermogravimetric analysis (TG-DTA) and temperature programmed desorption (TPD). Kinetic study of n-hexane over ZSM-5 catalysts is observed at temperatures of 500°C and 600°C under atmospheric pressure, mainly focusing the related reaction rate constants and activation energies. The n-hexane catalytic cracking was found to be first order regarding n-hexane concentration. The activation energies of 21.867 KJ/mol and 32.018 KJ/mol were evaluated for n-hexane over calcined and ion-exchanged samples. The application of ZSM-5 to the cracking of model naphtha is quite effective.

Table of Contents

List of Figures

Abbreviations

BTX	Benzene, Toulene, Xylene
DI	Deionized water
FCC	Fluid catalytic cracking
SDA	Structure directing agent
SS	Stainless steel
Si/Al	Silica/Alumina ratio
TPABr	Tetrapropyl ammonium bromide
TPAOH	Tetrapropyl ammonium hydroxide
TEOS	Tetraethyl orthosilicate
ZSM-5	Zeolite Socony Mobil–5

Chapter 1: Introduction

1.1 Background

Currently, Pakistan is experiencing one of its worst energy crises. Energy shortfalls are stumbling the economy and adding to the turmoil. In 2012, energy shortage was recorded at 58,00 MW but now it has peaked over 9,000 MW and by 2020, it is anticipated to rise above 10,000 MW [1][2]. In the present scenario, Pakistan needs to make crucial choices about energy consumption in the industrial sector and making strategies about the development of advanced, sustainable and renewable energy generation methods. This crisis can only be avoided if the Pakistani nation takes a serious step towards research and development.

The research work titled **"Fabrication of ZSM-5 and its ion exchange for naphtha cracking"** is all about developing zeolite based catalysts which are used for naphtha cracking. The main idea light olefins yield by reaction of ZSM-5 zeolite with light naphtha feed. Light olefins are the backbone of modern industrialization. At present, the petrochemical industry in Pakistan is very limited due to which most products are imported from foreign countries which takes a heavy toll on the import bill. The drastic change is going to happen to the industrial landscape by light olefins production. To boost up the economy of modern industrialization and fulfilling the global demands of petrochemical industries, zeolites and its additives are playing the crucial part by becoming the backbone and providing basic raw materials in the form of light olefins. The four major naphtha producing refineries in Pakistan are PRL (Pakistan Refinery Limited), ARL (Attock Refinery Limited), NRL (National Refinery Limited) and BYCO (Formerly Bosicor). Hence, there is, even more, need and the reason for the utilization of naphtha for the production of petrochemical products in which Pakistan is deficient.

1.2 An Introduction to the Petrochemical Industry

Petrochemicals refinery handles the chemicals and the products obtained from unrefined oil. A large stock of refined crude oil i.e. 90-95% can be utilized as a source of energy and basic materials are produced via the remaining oil. The origin of the petrochemical industry is described below with various examples in Figure1.

```
┌─────────────────────┐
│     Crude oil       │
└─────────────────────┘
          │
          ▼
┌─────────────────────┐
│    Oil Refinery     │
└─────────────────────┘
          │
          ▼
┌─────────────────────┐
│     Feedstocks      │
│                     │
│  Naphtha, Gas oil,  │
│    Natural Gas      │
└─────────────────────┘
          │
          ▼
┌─────────────────────┐
│  Chemical industry  │
└─────────────────────┘
          │
          ▼
┌─────────────────────┐
│   Basic chemicals   │
│                     │
│  Olefins, alkenes,  │
│     aromatics       │
└─────────────────────┘
          │
          ▼
┌─────────────────────┐
│    Petrochemical    │
│      industry       │
└─────────────────────┘
          │
          ▼
┌─────────────────────┐
│   Petrochemicals    │
│                     │
│  Synthetic fibers,  │
│    polyethylene,    │
│  polypropylene etc. │
└─────────────────────┘
```
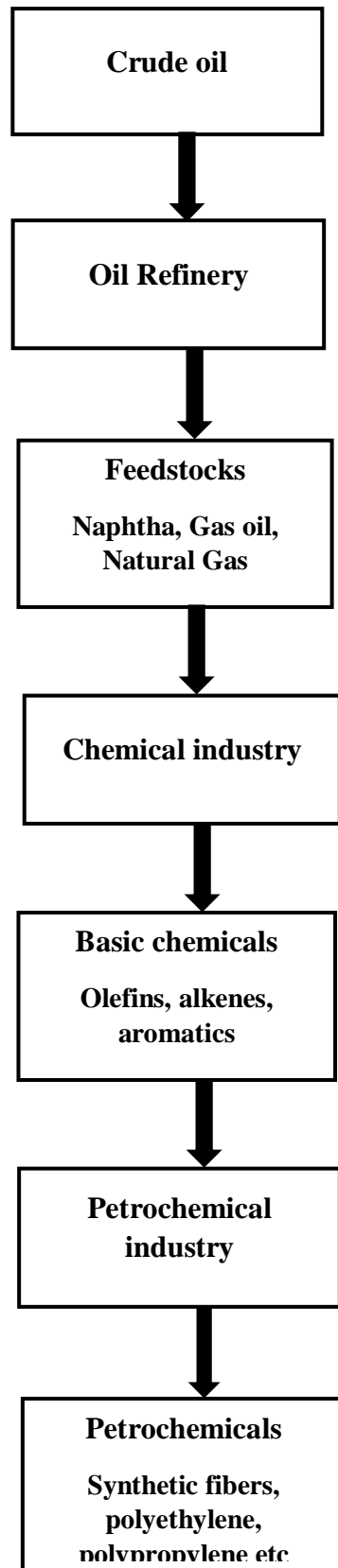
Figure 1. Origin of Petrochemical industry

The chemical industry is a vast industry giving the range of products from industrial gases, explosives to pharmaceuticals and food items. Petrochemical reactions are the chemical reactions involved in petrochemical processes. Some major petrochemical processes include;

1. Cracking

2. Reforming

3. Polymerization

4. Alkylation

5. Isomerization.

Thermal and Catalytic reactions are two major routes to accomplish above mentioned petrochemical processes. High-temperature conditions (400˚C to 1000˚C) are applied to thermal reactions, so high energy consumption occurs. This also poses a threat to uncontrolled heat. While catalytic reactions are highly appreciated because of their low power consumption and their requirement of low temperature and moderate pressure conditions [3].

1.3 An Introduction to Naphtha cracking

From the perspective of Sustainability and Environment security, nowadays there is much concern in replacement of essential energy asset petroleum by-products by alternative renewable energy sources. Energy and fuel source depletion has enhanced, extensively due to an abrupt increase in population. Due to lack of economic sustainability in a commodity market, alternative technologies are not preferable for investment in the chemical industry, regardless of the dangers of diminishing oil reservoirs and continuous increase in global warming [4]. Oil these days is the principle vitality origin and this prevailing condition most presumably will proceed in the following decades. The products produced by crude oil refining include naphtha, gas oil, and catalytic cracker gases. About 10% of oil refinery output by weight is naphtha. Crude oil refineries are basically designed for generation of petrochemical fuels along with economically feasible products like light olefins [5]. Naphtha is a petroleum fraction produced by lighter crude oil (<200ºC AET) which consists of molecules with 5-6 carbon atoms, with a boiling point between 20-80ºC. It is further fractioned into olefins and aromatics. Naphtha is

3

basically a mixture of alkanes, cycloalkanes and aromatic hydrocarbons [6]. Light olefins for example ethylene, propylene, butanes, and butadienes are essential raw materials for the petrochemical business and market of olefins is expanding each year. Olefins and BTX are the backbones of present-day life. Numbers of various derivatives used are produced from these building blocks. The several thermal processes developed in the early the 1960s are used for aromatics and the light olefins yield via crude oil cracking. These processes include; UBE process (47.8 wt. % of C_2-C_4 olefins) was developed at the end of the 1960s, BASF process (up to 40 wt. % of C_2-C_4 olefins), KK process in 1964 (22-32 wt. % of ethylene, 7-13 wt. % of propylene and 13 wt. % aromatics), Lurgi sand cracker (50.4 wt. % of olefins) and thermal regenerative cracking (22.5 wt. % of ethylene, 13.9 wt. % of propylene). BASF process main focus was to develop light olefins and BTX but without residue. Lurgi sand cracker and thermal regenerative cracking were designed for heavy oil. The other processes include Advanced Cracking Reactor, Dow process, Cracking Oil by Steam and Pascal cyclic thermal cracking [7]. Nowadays, petroleum-extracted naphtha cracking technique has mainly used the process for light olefins yield. For naphtha cracking in the petroleum industry, the hydro-cracking process is used while for the petrochemical industry steam cracking technique is used [5].

1.3.1. Thermal Cracking of Naphtha

The main technique used in naphtha cracking products is steam cracking. Steam cracking has been used for more than a half century. It is leading and well-established technology for light olefins production. Steam cracker used in thermal naphtha cracking consists of three main divisions: pyrolysis, fractionation/compression unit, and a product recovery/separation compartment. Pyrolysis compartment is an integral part of a naphtha thermal cracker, which is further divided into convection section, radiation section, and furnace draft. Pyrolysis occurs in the radiant section (temperature up to 1100°C). During pyrolysis, naphtha breaks down into free radicals by means of a free-radical mechanism, which further promotes the production of light olefins in gas form. Along with elevated temperature, low pressure and short residence time are also required for pyrolysis. From the fractionation section, fuel oil and BTX are obtained as products. Fouling and coking are the main problems related to this section. To avoid such problems several compartments of section required regular decoking. The pyrolysis section

utilizes the total process energy of about 65% and the total energy loss of 75%. The modifications are done in particular parts of naphtha steam cracker, but due to lack of economic and technical feasibility, most of them are not yet implemented [5]. However, steam cracking suffers from multiple limitations; highly energy-intensive process (requiring high temperature of about 800-1000ºC, and expensive construction materials), reporting about 40% of energy consumption every year in the entire petrochemical industry, difficult selectivity of specific light olefins and results in excess of CO_2 emission (about 180-200 million tons) and fouling issues by coke [8]. About 70% of light olefins is generated by thermal cracking [9]. During 2011, 94% of the world's propylene and 61% of ethylene in Asia, while in 2013, 95% of ethylene and 70-75% of propylene in Western Europe was supplied by thermal cracking.

1.3.2. Catalytic Cracking of Naphtha

The yield of light olefins via catalytic cracking as an alternative to steam naphtha cracking is classified into two major groups: acidic catalytic cracking and thermal catalytic pyrolysis. Acidic catalytic cracking is mostly related to proton donor acidic zeolites. It is also affiliated with Fluidized Catalytic Cracking or Fixed bed reactors and bulky raw materials while thermal catalytic pyrolysis requires naphtha feed and different types of metallic oxide based catalysts. Selectivity to desired products is greatly enhanced by catalysts [5]. In comparison to conventional steam naphtha cracking, catalytic cracking has high versatility in the feedstock and product slate is a less energy-intensive process (requiring a low temperature of about 550-650ºC). It suppresses the generation of carbon dioxide greatly, produces more olefins, and hence more economic value. Also, controlling the composition of olefins is quite easy. Catalytic cracking advances can prompt energy saving up to 20% [4]. Among catalytic cracking techniques in petroleum oil refineries, fluid catalytic cracking is among the prominent transformation innovations. The fluidized bed catalytic cracking units in petroleum refineries are the major source of light olefins. The main application of the FCC in an oil refinery is to convert low-value feedstocks into valuable items [7]. Mostly FCC catalyst consists of zeolite (active component, matrix (amorphous silica-alumina), binder and filler [10]. Zeolite FCC catalysts utilize lower activation energy for C-C bond breakage [5]. Typical FCC process derived ethylene yield of 2 wt. % and propylene yield of 3-6 wt. %. FCC process is

advantageous over steam cracking. For FCC process, no pretreatment for processing of unrefined petroleum is required [11]. The main requirements of the FCC process for a catalyst are; activity, selectivity, accessibility, attrition resistance, hydrothermal stability, metals tolerance, and coke selectivity [12]. For catalytic cracking, the two pathways utilized are mono-molecular and bi-molecular mechanisms. The mono-molecular mechanism is the main one involving chemisorption on the Brönsted acid sites to form carbenium ions which then cracked by beta scission to yield olefins. The bi-molecular pathway is a successive procedure, including the protonation of a double bond to form Penta-coordinated carbonium ions as a transition state. The carbonium ion expels methane to form a carbenium ion. The latter undergoes beta scission to form olefins [13]. Aitani et al. explained that the bimolecular cracking is not a favorable pathway for enhancing the manufacturing of olefin, which leads the hydrogen transfer reaction, where the olefin hydrogenation rate is prominent than paraffin dehydrogenation rate [14].

1.4 Importance of Light Olefins in the Petrochemical Industry

Since modern industrialization, light olefins have a dominant status. Globally, the demand for light olefins is quite higher than for some other chemicals. Olefins are used as feedstock for production of various industrial products such as synthetic fibers, construction materials, textiles, rubber and other chemicals in the petrochemical industry. Petroleum products, domestic and industrial fuels are mostly incorporated from fossil fuels. Nowadays, the utilization of energy is primarily done by refining, which is based on the combustion of fossil fuels [15]. Currently, for light olefins yield, feedstocks responsible are; crude oil and the ones obtained from natural gas. The crude oil is an ideal candidate by all accounts for the petrochemical field. It is economically available all over the world. Crude oil is also utilized as a part of the generation of gas, diesel fuel, and other important substances. Prominent olefins like ethylene and propylene are the monomers for polyethylene and polypropylene [15]. Unrefined crude oil is separated via distillation into a variety of consumer products like naphtha, gasoline, and kerosene, etc. Light naphtha is further fractioned for light olefins and aromatics production. Light olefins are key raw materials for a few of the most basic applications in the present plastic, pharmaceuticals, cosmetics, insulating products and synthetic fiber industry [5]. Light olefins have been produced by many

processes. The main production route is thermal naphtha cracking. With few shortcomings in steam catalytic cracking, catalytic naphtha cracking is considered a promising substitute. A large number of catalysts are used to enhance the selectivity of light hydrocarbons at the low-temperature range. Catalysts are basically the chemicals used to speed up the reactions. The reactions are completed in less time which means less energy is consumed. This is quite beneficial for industrial scale. On lab scale minimization of energy is quite insignificant while for large scale experiments it becomes important and catalyst usage also become compulsory. Importance of catalysis in the petrochemical industry is given below in Figure 2 [3]. Among the variety of catalysts, ZSM-5 zeolite as a catalyst has got a considerable measure of recognition. A number of hydrocarbon catalytic cracking experiments have been done over zeolitic ZSM-5 to explore the increasing chances of light olefins production.
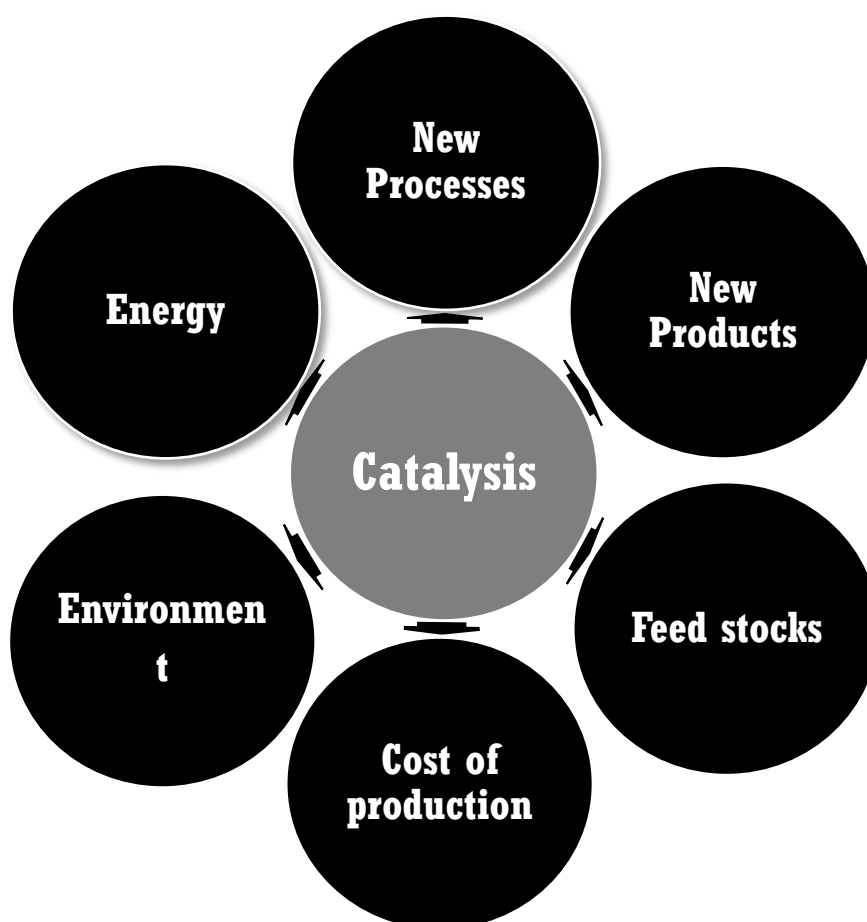
Figure 2. Catalysis impact on Process Industry

1.5 Catalysis History- Petrochemical Industry

The three major generations of catalyst while going through catalysis history are;

1.5.1 Generation I

Liquid acids like HF, sulfuric acid were initially used for accelerating petrochemical reactions. Their pros are;

1. Cheap

2. Effective

3. Easily available

While their cons include;

1. Corrosive Nature

2. No control over their activity during the reaction

3. Causes Environmental pollution if discarded carelessly

1.5.2 Generation II

Liquid acids were replaced with solid catalysts after extensive study. They were amorphous in nature. They have several advantages;

1. Easy handling

2. No environmental issue

3. No corrosion

4. Easy reaction control

While their disadvantages include;

1. Short catalyst life

2. Rapid deactivation

3. Difficult regeneration

1.5.3 Generation III

Generation III catalysts include crystalline solids. Crystalline aluminosilicates (Zeolites) were dominant among this generation's catalysts because of their high efficiency and long catalyst life [3].

1.6 Conventional Catalysts employed for Hydrocarbon cracking to light olefins

The present proficiency of refining and petrochemistry to a great extent is based on highly active, selective, and durable catalysts. The catalysts used for hydrocarbon cracking are generally grouped into acidic, basic and transition metal oxide catalysts. All three types are used under the aerobic or non- aerobic conditions [16].

Acidic catalysts (non-aerobic)

Examples are Ag-MOR/Al_2O_3, Cu/HZSM-5/P, and steamed HZSM-5. Performance parameters for naphtha catalytic cracking are; temperature range (550-650°C), yields of products (15-27 wt. % ethylene, 15-50 wt. % propylene, 11-34 wt. % aromatics).

Basic catalysts (non-aerobic)

Performance parameters for naphtha catalytic cracking are; temperature range (750-850°C), yields of products (30-40 wt. % ethylene, 15-22 wt. % propylene, 0 wt. % aromatics). Examples include CaO-SrO-Al_2O_3, WO_3-K_2O-Al_2O_3, and KVO_3/corundum.

Transition metal oxides/ basic catalysts (Aerobic/non-aerobic)

Operating parameters for naphtha catalytic cracking are; temperature range (500-800°C), yields of products (20-50 wt. % ethylene, 3-10 wt. % propylene). Cr_2O_3/Al_2O_3 is an example of a transition metal oxides/ basic catalyst [16]. A lot of research has been done on steam catalytic hydrocarbon cracking to produce desired light olefins. The catalyst used for naphtha cracking includes Oxide catalysts, Zeolite-based catalysts, carbon nanotubes based catalysts, and SAPO-34 based catalysts [17].

1.6.1 Oxide catalysts

Oxides catalysts for thermal catalytic cracking involve alumina catalysts, molybdenum oxide catalysts, calcium aluminates, and potassium aluminates catalysts. Aluminium oxide catalysts when modified, used in the temperature range of about 760-820°C. Oxides catalysts are modified with potassium carbonate and KVO_3 for naphtha cracking. Mukhopadhyay and Kunzru used potassium carbonate impregnated with Al_2O_3, which results in a depletion of the coke deposition and also

in amounts of methane and olefins (ethylene and propylene) [18]. Jeong et al presented the incorporation of KVO_3 with α-Al_2O_3 which showed increased production of ethylene by 10 wt. % and propylene by 5 wt. % [19]. Song et al experimented MoO_2 catalyst for n-hexane cracking in the temperature range of about 557-640°C. The final results showing the increase in light olefins selectivity in comparison to alkanes. In comparison to thermal cracking, α-Al_2O_3 spheres used for catalytic pyrolysis of naphtha in a quartz reactor resulted in enhanced production of ethylene and propylene by 1 wt. % and 5 wt. %. The coke deposition on the surface of the spheres increased due to the physical properties of α-Al_2O_3 spheres [20]. Pant and Kunzru investigated n-heptane steam pyrolysis by K_2CO_3 impregnated catalyst, which showed remarkable depletion in coke and minimal effect on product severity [21].

1.6.2 Carbon nanotubes based catalysts

An advantage of these catalysts is that the modification of carbon-based material is straightforward. Their high surface area, stability, excellent physio-chemical properties, higher reactivity, and resistance at high temperature make them a promising material in catalysis. The types of carbon nanotubes that are commonly employed are a single wall and multiwall [22]. In order to avoid its decomposition at temperatures higher than 500°C, carbon nanotubes should be covered with metallic oxides [23]. Grobert et al showed the modification of carbon nanotubes (CNTs) by coating them with SiOx. The results concluded that the resistance of catalyst to high-temperature increased [24]. Wang et al examined the impregnation of silicon on the carbon nanotube, which resulted in the initiation of a sample at 650°C [25]. Fu et al have also done the impregnation of silicon and their methods, which proved quite advantageous in silicon oxide thickness control [26]. Modification in carbon nanotubes by rare earth elements is studied by Keyvanloo et al for light olefins yield by thermal catalytic cracking of naphtha. The results concluded that the alteration of carbon nanotubes by a single layer of silicon increased its stability and production yields of ethylene, and propylene are enhanced by 26.5 wt. %. The total olefins production enhanced by 36.31 wt. % while maximizing the number of carbon nanotubes as a catalyst [27]. Sheibani studied Multiwall carbon nanotubes with different silicon layering. The carbon nanotube with 10 wt. % of SiO_2 at 680°C showed a maximum yield of ethylene (20.23 wt. %). The total olefin yield is above

250% of the amounts achieved via thermal cracking under the same conditions. Carbon nanotubes are an excellent candidate for naphtha cracking, but without modification with a silicon layer, they have very low stability toward high temperatures [28].

1.6.3 SAPO-34 based catalysts

Aluminophosphate molecular sieves (ALPO) are similar to aluminophosphate zeolites (SAPO) but their structures are a little bit different from each other, and ability of ALPO to be used as a catalyst is not very high. Among SAPO catalysts, SAPO-34 has high selectivity towards light olefins. The morphology of SAPO-34 is octagonal with a pore size of 3.5-6Å. The transformation of SAPO-34 crystals into aluminophosphate results in high acidity with increasing Silicon/Aluminum (Si/Al) ratio, which is quite the opposite of ZSM-5. SAPO-34 based catalysts have a large number of applications for MTO (Methanol to olefins) and ETO (Ethanol to olefins) [29]. Zhao et al studied the C_4-olefins catalytic cracking by using SAPO-34, HZSM-5, and H-mordenite. HZSM-5 catalyst reported the highest light olefins yield [30]. Selectivity of a number of zeolites for butane catalytic cracking was investigated by Zhu et al, which showed the high selectivity and high deactivation rate of SAPO-34 to light olefins [31]. In the case of naphtha catalytic cracking, the production rate of ethylene is greater with SAPO-34 but with a high deactivation rate that results in poor catalyst lifespan. In comparison to SAPO-34, H-ZSM-5 is excellent for naphtha cracking with a higher olefin yield and better catalyst lifespan [17].

1.6.4 Zeolites

The worldwide active catalysts used for naphtha cracking are solid proton-donating zeolites. They are quite significant key elements for petrochemical catalysis. In the early 1960s, zeolites were first introduced by Mobil. Microporous materials have a dominant field and as a part of such extensive discipline, zeolite applications have proceeded to develop strikingly in the modern world of chemical industries [32]. Acidic zeolite is vital to accomplishing high catalyst selectivity and activity to light olefins [33]. Zeolites are mostly used as catalysts and catalyst supports for a quite broad range of processes like petroleum refining, petrochemicals and pollution control [34]. According to the kinetic modeling studies, the rate of cracking of hydrocarbons changes with the nature of model compounds and zeolitic structure

[35]. Zeolites, being the model example of solid acids, possess a large surface area, higher stability, crystalline framework, high adsorption ability, and hydration-dehydration characteristics, which supports the development of environmentally benign processes [36]. Abrevaya et al reported the use of 8-12 member ring zeolitic catalysts for cracking of alkanes and naphthenes and verification of the connection between zeolite topography and cracking activity of naphtha. The maximum production of light olefins is attained using 10-MR zeolites. 12-MR zeolites lead to the bimolecular mechanism, which prompts the enhanced light paraffins and coke selectivity at the expense of light olefins [37].

Chapter 2: Literature Review

2.1 Introduction

Zeolites are commonly known as crystalline silicates or alumino-silicates and are linked via oxygen atoms which results in a three-dimensional network. The main attributes of zeolites are; tetrahedral arrangement, a pore framework, the presence of water, and charge compensating cations. Zeolites are widely applicable in the fields of catalysis, adsorption-separation, ion exchange, luminescence, electricity, magnetism, medicine, and microelectronics. Zeolites are of various types regarding shape, porosity, and composition. According to the silica/alumina ratio, zeolites can be categorized into three major classes.

1. Zeolites with low Si/Al ratio
2. Zeolites with moderate Si/Al ratio
3. Zeolites with high Si/Al ratio

For a selection of catalyst, the Si/Al ratio plays a significant part in a reaction.

2.2 Crystalline Microporous materials: Zeolites

International Union of Pure and Applied Chemistry (IUPAC) have sorted the zeolites in three main groups regarding their pore diameter.

1. Microporous zeolites (having diameter < than 2 nm)
2. Mesoporous zeolites (having diameter > than 2 nm but < than 50 nm)
3. Macroporous zeolites (having diameter > than 50 nm) [38].

2.3 Timeline of development of Zeolites

In 2009, Soni et al published the timeline of usage of zeolites in the production of higher FCC olefins is; Development of ZSM-5 in FCC (1970), invention of Zeolite Ultrastable Y in FCC (1974), Commercialization of ZSM-5 in catalytic cracking (1983), Development of Zeolite Beta in Fluid catalytic cracking (1986) and first olefin production via ZSM-5 (1990) [39].

2.4 Synthesis and catalytic activity of ZSM-5 Zeolite

2.4.1 ZSM-5 Zeolite

In 2002, Corma et al showed the catalytic activity of ZSM-5 (10MR), owing to the high surface activity, structure selectiveness, ion-exchange characteristics, specific three-dimensional pore topology, and large surface area. ZSM-5 is dedicated to producing other 10 Membrane ring pore zeolites (ZSM-22, Theta-1, ZSM-35, ferrierite) which possess uni-dimensional pore topology with catalytic limitations of diffusion and pore plugging. The catalytic activity of these zeolites is lower in comparison to ZSM-5 [40].Kubů et al, in 2010, investigated the parameters affecting the synthesis, characteristics, and acidity of zeolites such as TUN, IM-F and -SVR in comparison to MFI (ZSM-5). The synthesis of-SVR is done with Silica-Alumina ratios over than 100. MF-I is synthesized by a Si/Al ratio of about 65.4 while for TUN and IMF Si/Al ratio is about 20-30. The results concluded that the acidic features of all three zeolites are the same regarding their acidic nature and Bronsted/Lewis acid site ratio [41]. Garforth et al, in 2015, reported the different zeolite structures; ZSM-5, Ferrierite, and Beta catalyst and their role as FCC additives for increasing the yield of propylene via n-heptane cracking. All of these zeolites have entirely different structures. ZSM-5 have bi-directional 10-Membrane ring pathway, Ferrierite with bidirectional 10×8 Membrane ring pathway framework, and Beta Zeolite have tri-directional 12-Membrane ring channels. The reaction involved in n-heptane cracking is quite complex. Its mechanism involves monomolecular and bimolecular cracking. Conventional ZSM-5 and nano ZSM-5 showed higher catalytic activity of about 90 mol. % in comparison to Beta (5-60 mol. %), and Ferrierite (20-40 mol. %). Addition of Beta with ZSM-5 improved its catalytic activity as well as propylene yield. At higher temperature, the highest yield of propylene is obtained over only Beta zeolite. The residence time has a negative impact on ZSM-5 and Ferrierite, and no effect on Beta zeolite. Nano ZSM-5 is proved to be as the best option for FCC additive while the results reported that Beta zeolite supports bimolecular cracking (hydrogen transfer reactions). The catalytic activity of ZSM-5 is higher and have low selectivity towards hydrogen transfer [42]. Seyed Mojtaba, in 2016, reported that ZSM-5 and other pentasil-ring zeolites can be added as additives to the cracking units for maximization of light olefins yield.

Different synthetic zeolites like ZSM-5, zeolite USY, zeolite X, zeolite ZK-5 etc and naturally occurring zeolites as for example chabazite, faujasite, mordenite can be considered as a good option for naphtha catalytic cracking [13].

2.4.2 Catalytic Activity of ZSM-5 Zeolite for Naphtha Cracking

In 2010, Al-Khattaf et al discussed the catalytic cracking of naphtha over mesoporous ZSM-5 and its role for the enhancement of light olefin production. The catalytic activity of meso-ZSM-5 is compared with traditional ZSM-5 with varying Si/Al ratio. The surface area of mesoporous ZSM-5 is higher than conventional ones. The propylene yield of 16 wt. %, ethylene yield of 10 wt. % and BTX yield over meso-ZSM-5 are also higher than the conventional one. The main reason for this is meso-ZSM-5 lower HTI (Hydrogen Transfer Index) [11]. Ramin Karimzadeh and Nazi Rahimi published their review, in 2011, on hydrocarbons cracking over modified ZSM-5 zeolites. This paper reviewed the yield of light olefins through cracking of numerous hydrocarbons over zeolite which is modified with various promoters. In early research, zeolites result in lower ethylene yield but higher propylene and aromatic yields. In case of naphtha cracking over ZSM-5 modified with La results in higher yield of olefins as well as aromatics but BTX yield can be reduced by incorporation of ZSM-5 with phosphorus, magnesium, copper, and calcium. ZSM-5 modification with cobalt, iron, zinc, and nickel decreases light olefins yield but also suppresses the BTX and coke yields. The incorporation of fluorine in ZSM-5 is quite effective for naphtha cracking and positively affects the pore framework of the catalyst by enhancing the light olefins yield. Pore topology and acidity of zeolite are the key components in catalytic cracking as they greatly affect the conversion and product yields. Cracking of paraffin over ZSM-5 leads to dealumination and lower activity. ZSM-5 modification with rare earth elements, and phosphorous results in enhanced light olefin selectivity and yield. The phosphorous modification also results in acidity which in return provides a path for enhanced light olefins production [34]. In 2013, Tago et al studied the catalytic cracking of n-hexane and n-heptane over ZSM-5 catalyst. The macro and nano ZSM-5 catalysts were compared for their cracking activity of n-hexane. Conversion of n-hexane at 550°C, 600°C, and 650°C without catalysts were 1.2%, 4.8%, and 20%. Products like alkanes, alkenes, and aromatics were obtained via n-hexane cracking. The increased in temperature enhanced the selectivity of light olefins and BTX while selectivity of

paraffin decreased. The high temperature of about 650°C lowered the acidity of catalyst (high Si/Al) which favored the high yield of olefins i.e. 50.4%. The nano and macro ZSM-5 having the same acidity showed the same initial n-hexane conversion of 83% [43]. In 2014, Tago et al discussed the catalytic cracking kinetics of naphtha cracking over macro and nano HZSM-5 in the temperature range of about 475-650°C. In comparison to nano ZSM-5, a lower olefins yield is obtained by macro ZSM-5. Nano ZSM-5 exhibited higher olefins yield (57 mol. %) and catalytic activity. The coke yield by macro ZSM-5 (17 wt. %) is quite higher than nano ZSM-5 (2.9 wt. %). The activation energy and reaction rate constants for nano zeolite are quite higher than micro ZSM-5. The rate constants for naphthenes (cyclohexane, methylcyclohexane) are lower when compared with n-hexane. But for activation energy opposite happened. The activation energy of n-hexane (126 kJ) is higher than activation energies of CH (119 KJ) and MCH (116 kJ) which proved reactivity of naphthenes is quite higher than alkanes. Diffusion limitations of macro zeolite were 400 times greater than nano zeolite [44].

Li et al, in 2015, published his work on the synthesis of zeolite using natural aluminosilicate mineral such as diatomite. The resultant ZSM-5 zeolite has high hydrothermal stability which is then used as an additive to the FFC catalyst. The composite (ZSM-5/FCC catalyst) showed high propylene (1.66 wt. %), selectivity, light olefins yield (2.36 wt. %), and low coke selectivity (1.54 wt. %) in comparison to as synthesized FCC catalyst [45]. Shayan Alipour, in 2016, published a review on catalytic cracking of naphtha via nano ZSM-5. He discussed the effect of nanosized ZSM-5 on different parameters like conversion, catalytic activity, selectivity, and catalyst lifespan and compared it with micro-ZSM-5. The impact of the type of feedstock and temperature were also described and highlighted how they improved the conversion and selectivity of light olefins (47.9 wt. % to 76.1 wt. %). In the case of micro ZSM-5, the catalytic activity of the catalyst is hindered by many limitations regarding its applications in naphtha cracking. The main reason is the highly acidic nature of zeolite which results in coke generation which further leads to a decrease in catalyst lifespan and finally in the deactivation of zeolite. Due to which diffusion process within the micropores is quite limited. To overcome this problem the only possible solution is to reduce the catalyst size from micro to nano. Nano-ZSM-5 application notably improved the deactivation rate, catalyst lifespan, and catalytic

activity. Nano-ZSM-5 shows high selectivity for light olefins and low selectivity for BTX in comparison to micro zeolite. Nano ZSM-5 shows encouraging results for naphtha cracking reactions [13]. Corma et al, in 2017, discussed the FCC catalysts used for maximum light olefins production. Zeolite Ultrastable Y (USY) gives the highest yields of ethylene and propylene. It produces less coke but has low stability. MCM-41 also shows low thermal stability. MCM-22 has a higher selectivity for light olefins than ZSM-5 but lower activity. In the case of Zeolite Beta, there is a higher yield of ethylene but it is very costly with poor stability. The pore framework of Zeolite ITQ-7 is quite identical to Zeolite Beta with improved olefin selectivity. Cracking activity of ZSM-20 and Zeolite ITQ-21 is similar to Zeolite Y. ZSM-5 gives an excellent propylene yield, but with an additive dilution effect. The advantage of using ZSM-5 is its medium pore which can diminish the coke formation due to lack of large openings in the pore structure and low density of acidic sites [7].

Ji et al, in 2017, reported the study on n-dodecane catalytic cracking over phosphorous modified ZSM-5 zeolite. Phosphorous contents of about 0.5, 1, 2, 3 (wt. %) was incorporated into ZSM-5. Then their effect on stability and catalytic activity of ZSM-5 was evaluated. XRD results showed that crystallinity of zeolite decrease with the increasing phosphorous amount. The pore volume and BET surface area also decreased with a rise in phosphorous content. The deactivation rate of modified zeolite decreases, the density of acidic sites decreases, catalytic activity and yield of light olefins increase with an increase in P-content. The optimum amount is 0.5 wt. % at which the maximum yield of olefins, alkene selectivity, catalytic activity, and stability of zeolite is achieved. Modified ZSM-5 zeolite showed enhanced n-dodecane cracking than parent ZSM-5 zeolite [46]. In 2017, another paper about phosphorous modified ZSM-5 enhancing the hydrothermal stability for catalytic cracking of olefin was published by Guo et al. P-modified ZSM-5. Phosphorous contents of about 0.2, 0.6, 1, 2, 3 (wt. %) was incorporated into ZSM-5. The optimum amount is 1 wt. % at which the maximum yield of olefins, alkenes selectivity, and catalytic activity of zeolite is achieved. As a modifier precursor $(CH_3)_3PO_4$ is much better than $NH_4H_2PO_4$. Yields of C_2-C_4 olefins and gas increased by 35% and 38% in comparison to parent ZSM-5 (23%, 25%) [47]. Liu et al, in 2017, studied the effects of regenerated parent ZSM-5 and Ag/ZSM-5 in n-pentane catalytic cracking for light olefins yield. Hydrogen and ethylene selectivity is higher

for regenerated ZSM-5 than parent ZSM-5. The regeneration process requires high temperature which leads to a decrease of Bronsted acidic sites in ZSM-5 and results in low P/E ratio, enhanced selectivity, and the yield of light olefins. Parent ZSM-5 achieved light olefins selectivity of about 55 wt. % which is 25% less than what achieved by regenerated Ag-ZSM-5 (69 wt. %). While for Ag-ZSM-5 it is 13 wt. % less in comparison to regenerated Ag-ZSM-5 [48]. Widayat et al, in 2017, reported his work on the synthesis of ZSM-5 as a catalyst at 200°C for 6 and 8 hours and then calcination treatment of as-synthesized samples at various temperatures in the range from 500°C-800°C is carried out. He discussed temperature and crystallization time effect on the morphology and crystallinity of ZSM-5. Enhancement in crystallization time guides to a compact ZSM-5 catalyst framework and enhanced crystallinity of catalyst. The catalyst crystallinity at 6 hours is 33.35%, while for 8 hours (34.33%). After calcination at different temperatures, synthesized ZSM-5 catalyst has amorphous morphology and its crystallinity decreases in comparison to conventional ZSM-5 catalyst (76.1%). In general, the crystallinity of synthesized ZSM-5 increases with increase in temperature. The crystallinity values at different temperatures are; 500°C (39.2%), 600°C (44.1%), 700°C (42.9%), and 800°C (44.9%) [49]. In 2018, Wu et al. reported the enhancement in selectivity of propylene for butylene catalytic cracking over WZSM-5. W-ZSM-5 with a 45-mole ratio showed the highest yield of propylene (37 wt. %), conversion (96 wt. %), total propylene and ethylene yields (55 wt. %) and highest hydrothermal stability [6].

2.5 Aims and Objectives

2.5.1 Aim of Project

Petrochemicals are the backbone of modern industrialization. At present, Pakistan lacks the naphtha cracker. Due to which the naphtha cracking research and petrochemical industry are very limited and most of the products are imported from foreign countries which takes a heavy toll on the import bill. Petrochemicals production in the country is going to change the industrial landscape. To boost up the economy of modern industrialization and fulfilling the global demands of petrochemical industries, zeolites and its additives are playing the crucial part by becoming the backbone and providing basic raw materials. Nowadays, the development of stable and enhanced petrochemicals yield is the main focus. This

project is all about developing zeolite based catalysts which are used for n-hexane naphtha cracking. The main purpose is petrochemicals yield by doing the cracking of model naphtha feed over ZSM-5 catalyst.

2.5.2 Objectives

In this research work, we are comparing the catalytic activity of calcined ZSM-5 and ion-exchanged (HZSM-5) zeolite samples for model naphtha (n-hexane). In the already published literature, mostly catalytic cracking is done by HZSM-5. Up till now, no one did the kinetic study of both samples for n-hexane. But in this study, we are using a calcined sample as well to see the difference in the catalytic activity of both zeolite catalysts at the same temperatures.

1.   Synthesis of calcined and its ion exchanged ZSM-5 zeolite catalysts

2.   Characterization of synthesized ZSM-5 zeolite samples

3.   Catalytic activity analysis of calcined and its ion exchanged ZSM-5 zeolite samples using model hydrocarbon.

Chapter 3: Materials and Methods

The main objective was to obtain zeolitic ZSM-5 via hydrothermal crystallization techniques. The general schematic for the description of H-ZSM-5 synthesis is given in Figure 3. The stepwise description of each technique is described below.

3.1 Materials used

Celite$^@$ 545, Sodium hydroxide and Tetraethylorthosilicate were purchased from MERCK KGaA. Tetrapropylammonium bromide (purity >98%) and Tetrapropylammonium hydroxide (1M aq. soln) were purchased from Alfa Aesar. Sodium aluminate (DAEJUNG) used as silica and alumina sources. Ammonium chloride and Ammonium nitrate were purchased from DAEJUNG Chemicals. For centrifugation and washing, absolute ethanol was used (LAB SCAN Analytical Sciences). Deionized and distilled water were used as a solvent.

3.2 Synthesis technique of ZSM-5 Sample A

Firstly calculated amounts of Celite-545, sodium aluminate, and tetrapropylammonium bromide were mixed in deionized water. The pH of the solution was noted as 13 under continuous stirring by using sodium hydroxide. After vigorous stirring at ambient temperature for about an hour, the resultant mixture was poured into stainless steel autoclave with Teflon lining for 50 hours at 170°C in the oven. The sample obtained after hydrothermal synthesis were centrifuged at 4500rpm for 30 minutes, then washed with deionized water for about 3-4 times and finally dried at 110°C overnight. After drying, the sample was crushed into powder form and then calcination occurs for 5-6 hours at 550°C. The organic template of the as-synthesized sample was decomposed after calcination. Na-ZSM-5 sample was ion-exchanged thrice with aqueous NH_4Cl at 80°C for 2 hours to obtain HZSM-5. This was followed by centrifugation at 4500rpm, three times washing, and overnight drying at 110°C. After final ion-exchanged, the sample was calcined at 550°C for 5 hours[45].

3.3 Synthesis technique of ZSM-5 Sample B

Firstly, 4.9g of NaOH was added in deionized water to give 99.7g of solution I. Solution II was obtained by the addition of 18g of Celite$^@$ 545 into solution I. Then

7.4g of tetrapropylammonium bromide was added to obtain the raw material. The resultant mixture was poured into stainless steel autoclave with Teflon lining for 20 hours at a crystallization temperature of about 180°C in an oven. The sample obtained after hydrothermal synthesis were centrifuged at 4500rpm for one hour, then washed with deionized water for about 3-4 times and finally dried at 110°C overnight to obtain pure phase. After drying, the sample was crushed into powder form and then calcined at 550°C for 5 hours [50]. The calcined sample was then ion-exchanged with 1M NH_4NO_3 thrice for about 2-3 hours at 80°C under reflux [51].

3.4 Synthesis technique of ZSM-5 Sample C

3.4.1 Preparation of silica

First of all solution, I was prepared by mixing calculated amounts of absolute ethanol, aqueous ammonia, and deionized water. The solution I was stirred for about 5 minutes. Solution II was prepared by addition of 5ml tetraethylorthosilicate into 30ml absolute ethanol. Then Solution I was added into Solution II under stirring. The reaction proceeded for 24 hours at 25°C. This was followed by centrifugation at 4500rpm, thrice ethanol washing, and drying at 110°C for 2 hours [52].

3.4.2 Preparation of colloidal silica

1.365 grams of silica was added to 8.635 grams of distilled water.

3.4.3 Process details

Firstly, calculated amounts of sodium aluminate, tetrapropylammonium hydroxide, and sodium hydroxide were dissolved into 32.5ml of distilled water to obtain a resultant mixture. Then the drop wise addition of 1.365g of colloidal silica to the resultant mixture is done under continuous stirring. After vigorous stirring at ambient temperature for about 3 hours, the resultant mixture was poured into stainless steel autoclave with Teflon lining for 48 hours at 120°C in the oven. The sample obtained after hydrothermal synthesis were centrifuged at 4500rpm for 1 hour, then washed with distilled water for about 3-4 times and finally dried at 120°C for 5 hours. After drying, the sample was crushed into powder form and calcined at 550°C for 6 hours. C-ZSM-5 sample was ion-exchanged thrice with aqueous 1M NH_4NO_3 to obtain HZSM-5 [53].

```
┌──────────────┐      ┌─────────────┐      ┌──────────────┐
│  Celite@545  │─────▶│  Distilled/ │◀─────│  TPAOH/TPABr │
└──────────────┘      │  Deionized  │      └──────────────┘
                      │    water    │
                      └─────────────┘
                             │
┌──────────────┐      ┌─────────────┐      ┌──────────────┐
│    Sodium    │─────▶│   Mixing    │◀─────│   Magnetic   │
│   hydroxide  │      └─────────────┘      │   Stirring   │
└──────────────┘             │             └──────────────┘
                             ▼
                      ┌─────────────┐
                      │  Hydrolysis │
                      └─────────────┘
                             │
                             ▼
                      ┌─────────────┐
                      │Crystallization│
                      └─────────────┘
                             │
                             ▼
                      ┌─────────────┐
                      │ Filtration and│
                      │   Washing   │
                      └─────────────┘
                             │
                             ▼
                      ┌─────────────┐
                      │   Drying    │
                      └─────────────┘
                             │
                             ▼
                      ┌─────────────┐
                      │ Calcination │
                      └─────────────┘
                             │
                             ▼
                      ┌─────────────┐
                      │Ion-exchanging│
                      └─────────────┘
                             │
                             ▼
                      ┌─────────────┐
                      │ Calcination │
                      └─────────────┘
```
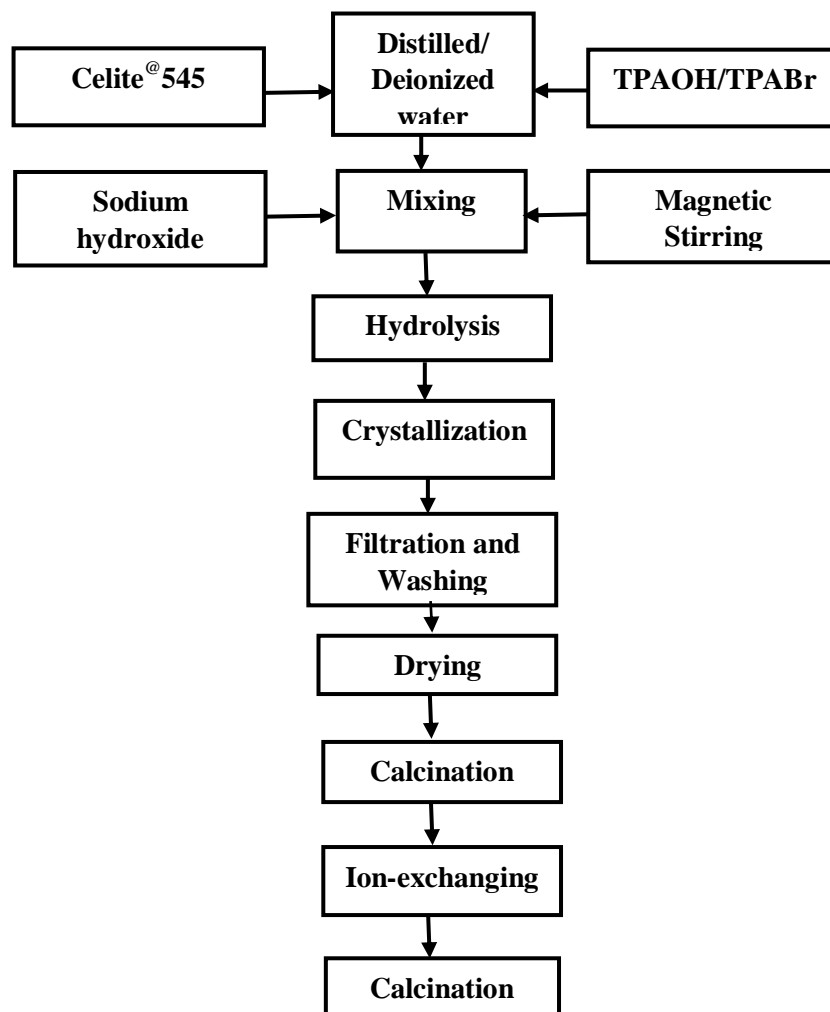
Figure 3. Synthesis diagram of H-ZSM-5 Zeolite Samples

3.5 Catalytic cracking of n-hexane

Catalytic cracking of n-hexane over different ZSM-5 catalysts was conducted using Stainless steel (SS) microreactor- Packed bed reactor (PBR) at reaction temperatures of about 500°C and 600°C under atmospheric pressure. First powdered catalysts were compressed under load and then after further crushing they were converted in sieves to maintain porosity and were placed in the PBR. Before each run, catalysts were activated for about 1 hour under N_2 flow. After activation of the catalyst, n-hexane in the liquid phase with nitrogen (carrier gas) was introduced in the reactor via the inlet. The value of F is 0.5mol/hr and is constant. Variation in the amount of catalyst resulted in different catalyst weight/feed rate (W/F) ratios. The initial

22

concentrations of n-hexane are known while final concentrations of n-hexane were calculated at the reactor outlet. In Table 1, the specifications of the microreactor are given.

Table 1. Specifications of the microreactor

Stainless Steel Microreactor	Specifications
Internal Diameter (ID)	8 mm
Height (H)	280 mm
Catalyst amount	10 mg
Catalyst Pore size	40-60 mesh size
Volumetric Flow rate of n-Hexane	11 ml/min
Weight Hourly Space Velocity (WHSV)	2-6 hr^{-1}

3.5.1 Packed bed reactor (PBR)

For catalytic processes, packed bed reactors (also known as plug flow reactors or fixed bed reactors) are mostly used reactors in the chemical industry. They are the type of heterogeneous reaction systems. The catalyst in the form of pellets or sieves is placed in the chamber and liquid/gas flow across it which results in the alteration of chemical composition and generation of products. In comparison to other reactors, they give the highest rate of conversion per weight of the catalyst. They are used for both liquid and gaseous phase reactions. The flow of the fluid through PBR is considered as a plug flow, which is an idealized flow with the same velocity for every particle involved in the flow and also they have an identical direction of motion. This reactor involves very little or no back mixing and also provides very good contact between fluid and catalyst which is quite advantageous. They are not expensive and require low operating cost and are highly efficient at elevated

pressures and temperatures. They are preferable over other reactors regarding their conversion. The schematic of the packed bed reactor is given below. PBRs are applicable in a wide range of chemical processes including separation, absorption, stripping, catalytic reactions and distillation [54][55].
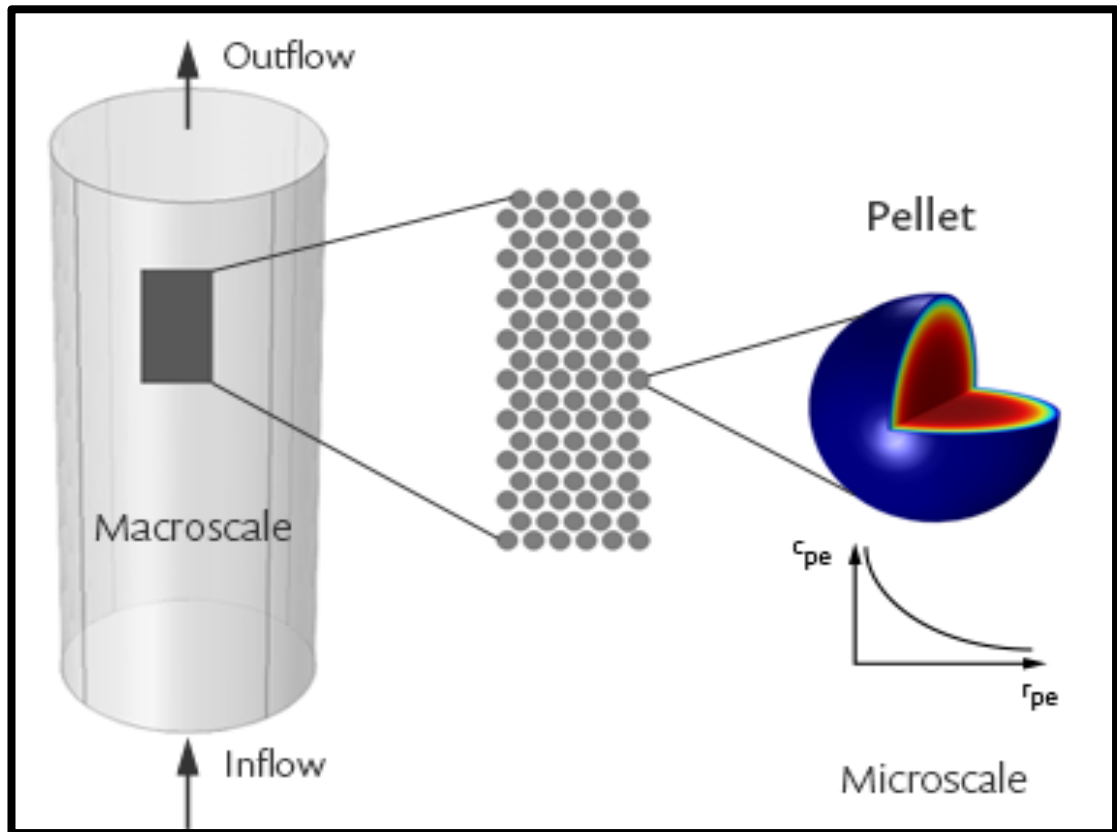

Figure 4. Schematic of packed bed reactor

Chapter 4: Characterization Techniques

The characterization of calcined ZSM-5 zeolite and modified ZSM-5 zeolite samples is done by various techniques; XRD, SEM, FTIR, TG-DTA, and TPR. These techniques are discussed below;

4.1 X-ray Diffraction analysis (XRD)

X-ray diffraction technique high lightened the study of polycrystalline phases and crystalline structures of solid materials. Around 95% of solid materials are reported as crystalline. XRD method is ideal for the identification and analyzing unknown phases. It is a highly nondestructive technique used for characterization of an extensive range of materials involving catalysts, pharmaceutical products, polymers, ceramics, minerals, and metals etc. XRD basically depends upon the interaction of monochromatic radiation with the crystalline sample. Thus, the XRD pattern is obtained by the constructive interference of X-rays with a crystalline substance, which is quite like a fingerprint of substance used for recognition. It provides valuable information about lattice parameters like average spacing between atoms, strain orientation of crystals, phase composition, internal stress, unit cell dimensions and crystalline structure of unknown phases. X-ray diffraction requirements involve single wavelength radiation. The working principle reports that monochromatic X-rays generation is based on high energetic electron beam and when it is accelerated towards copper or molybdenum surface by application of voltage and bombarded it with electrons, which will, in turn, evict the inner shell electrons and results in the production of X-ray spectra. Following equation tells the relationship between the energy of radiation and wavelength;

$$E= hc/ʎ \qquad\qquad (1)$$

Where h is planks constant and c is the speed of light in vacuum. Then these X-rays are directed towards sample which will result in constructive interference and a diffracted ray. The diffracted X-rays are then processed and counted. Working Principle of X-ray diffraction is given below in Figure 4. For the identification of an

unknown compound, diffraction peaks are converted into d-spacings. Each and every compound has its own particular d-spacings set. The scanning of a sample by X-ray diffractometer is done through whole 2θ angles range. Bragg's law is used for understanding the X-rays diffraction pattern.

$$n\lambda = 2d\sin\theta \qquad (2)$$

This law depicts the relationship between the diffraction angle and the wavelength of electromagnetic radiation. It also gives insight into the interplanar spacing of the crystalline sample [56].
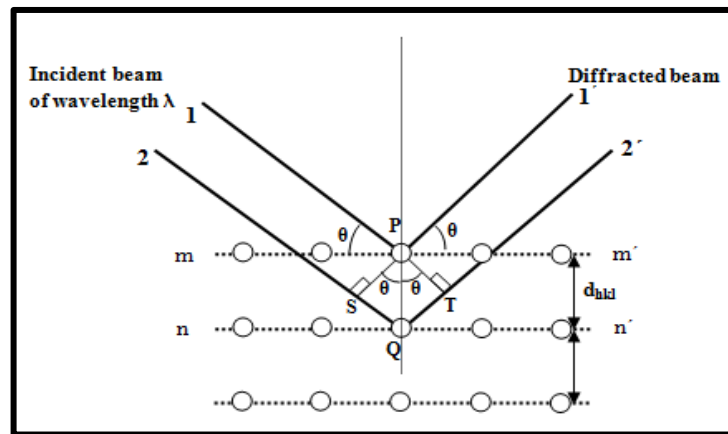
Figure 5. Working principle of X-rays diffraction analysis

4.2 Scanning electron microscope analysis (SEM)

Analysis of morphology and composition of the materials is very important regarding the study of nanomaterial. For observation of morphology and surface of materials, the scanning electron microscope is a powerful instrument to provide high spatial resolution results. SEM is also called an electron microscope. Both SEM and light microscope works on the same principle, but for magnification of objects, SEM utilizes a beam of electrons instead of photons. Study of SEM images provides both qualitative and quantitative information. And it also requires simple sample preparation [57]. The scanning electron microscope generates raster pattern by scanning surface images of the sample with a high energy beam of an electron. The working principle of SEM involves the interaction of high energy beam of the electron generating from electron gun with the surface of a sample, which results in the production of secondary electrons, primary backscattered electrons, and X-rays. SEM utilizes only secondary electrons and primary backscattered electrons. Both

types of electrons give information about chemical composition, morphology and surface topography. But backscattered electrons are more concerned about rapid phase discrimination. The electron-sample interactions result in high resolution three dimensional black and white images with image magnification up to 10nm. The working rule is also displayed in below Figure 5. SEM imaging is classified into three categories;

1.   Non-random, time-independent spatial distortion

2.   Non-random, time-dependent distortion

3.   Random, time-dependent distortion [58]

One of the SEM's most noteworthy points of interest is its ability to recreate printed data in a very steady and coherent way [59].
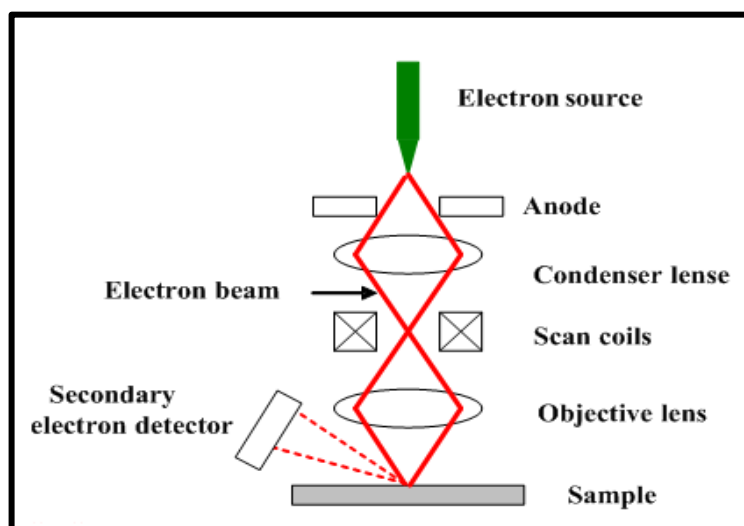

Figure 6. Working principle of the Scanning electron microscope

4.3 Fourier-transform infrared spectroscopy (FTIR)

FTIR is a powerful experimental tool used for the identification of molecular structures, chemical bonds and provides information regarding quantitative and qualitative analysis of inorganic and organic samples. It determines the chemical bonding via production of infrared absorption spectrum which is more like an individual molecular fingerprint of each component. Each and every kind of bond has its own distinctive infrared frequency. The electromagnetic absorption spectrum lies in infrared region of $4000cm^{-1}$-$200cm^{-1}$. This spectrum is further divides into fingerprint (1400-$600cm^{-1}$) and functional group (4000-$1400cm^{-1}$) regions. It is a

powerful analytical tool used for detection of the functional group. It has been effectively applied for the broad range of applications like;

1. Screening of impurities and toxicity

2. Analysis of pharmaceuticals, metals, polymers, paints, coatings, plastics, enzymes, amino acids and proteins etc.

3. Analysis of contamination

4. Analysis of unknown compounds [60]

The basic working rule of FTIR is well founded on the interaction between the electromagnetic radiations and samples which are in the possession of induced or permanent dipole moment and excitation of various vibrational levels. The different basic parts of FTIR spectrometer consists of; Infrared source, an interferometer, sample, detector, interferogram, FFT computer (signal processor). When infrared radiation beam is targeted to a sample, radiation is absorbed at various frequencies correspondence of molecular vibrational frequencies but also results in the transmission of other frequencies. Firstly, radiation passed through interferometer where almost all of the radiations are measured simultaneously. The beam passing via interferometer results in interferogram due to constructive and destructive interference. Then radiation beam passes through sample division where it is absorbed at particular frequencies showing its unique characteristics. The resultant plot in the form of an IR spectrum is obtained between transmittance (%) and wavenumber (cm^{-1}). In the end, detector measure interferogram signal in binding energy vs time. The Fourier transformation occurs at FFT computer which is further presented for interpretation. The working principle is also shown in below Figure 6 [61].
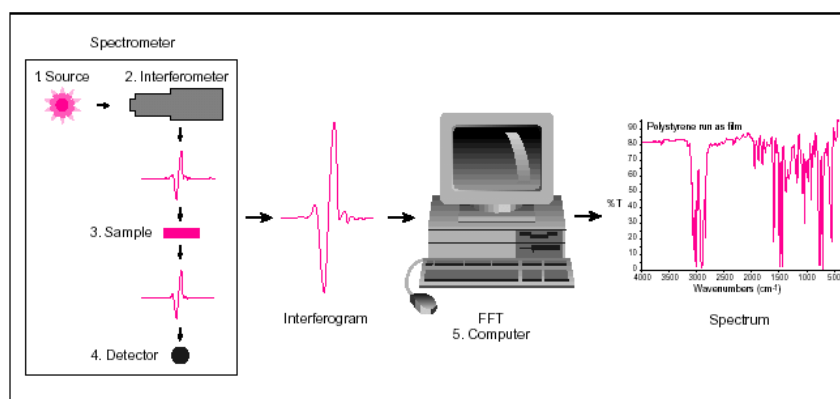
Figure 7. Schematic diagram of Fourier-transform infrared spectroscopy

4.4 Differential thermogravimetric analyzer (TG-DTA)

Differential thermogravimetric (TG-DTA) analysis is referred to as thermogravimetric and differential thermal analysis simultaneously. Thermogravimetric (TG) offers information regarding a variation in physical phases including absorption, sublimation, adsorption, vaporization, and desorption etc. It is an analytical technique which gives measurements regarding the variation in mass (loss or gain) of the sample as a function of time/temperature. It is applied for the various applications like analysis of chemical kinetics, determination of sample's purity, moisture amount, thermal stability of material and de-compositional behavior analysis [62]. While differential thermal analysis (DTA) provides data related to phase transitions like sublimation, melting point, glass transitions and crystallization (no weight loss occurs). When the sample is heated, the reaction start and sample undergoes phase transformation which is resulted in heat emission and absorption. This analytical technique is used for the identification of the sample's chemical composition by monitoring the difference in temperature between the sample and reference sample plotting vs temperature. DTA technique is widely applicable to various fields like; pharmaceuticals, environmental research, metallurgy, and inorganic chemistry [63]**.** The basic principle of TG.DTA works on the combined application of both TG and DTA. A differential thermogravimetric analyzer (TG/DTA) combines both analytical techniques and applies them to a single sample in a same analyzing instrument under controlled measuring conditions (gas atmosphere, flow rate, heating rate, and vapor pressure etc.). Differential thermogravimetric analysis is applicable for the determination of reaction rate along

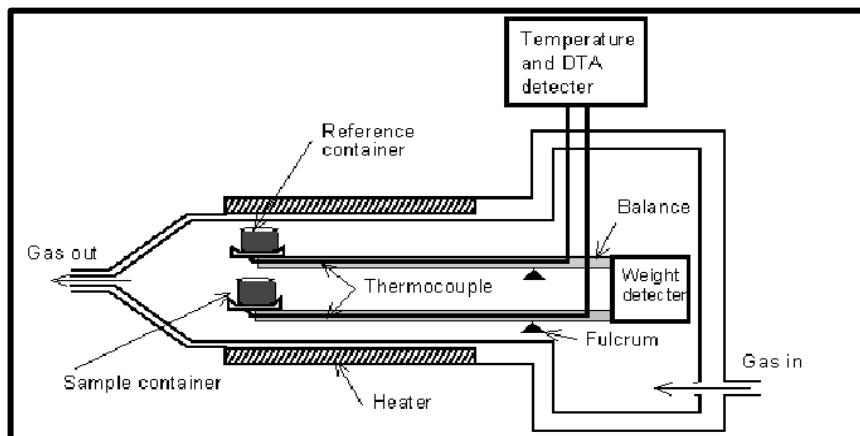with the combined applications of TG and DTA. Figure 7 shows the schematic diagram of TG/DTA [64].

Figure 8. Schematic diagram of Differential thermogravimetric analyzer

4.5 Gas chromatography-mass spectrometry (GC-MS)

Gas chromatography-mass spectrometry (GC-MS) is an analytical technique originated from a combination of both gas chromatography (GC) and mass spectrometry (MS). This technique is highly appreciated for unknown elements identification. GC/MS is also used for analyzing complex chemical mixtures (biochemical or organic) and environmental specimens. Individually, gas chromatography efficiently separates compounds but cannot do elemental analysis and for mass spectrometry, it can quantify and differentiate the elements (comprehensive morphological details) but cannot separate them. Both techniques are extremely compatible with each other. The mass spectra generated from GC-MS provide a lot of structure associated information. This can be done by studying ions fragmentation. GC/MS analyzer consists of different compartments such as injector, gas chromatography column, oven, ion source, mass spectrometer, a mass analyzer, detector and finally electronics control. The working principle of GC/MS works on coupled functioning of both GC and MS sections. In the GC section, at first, the sample is introduced through the injector and is heated in a gas chromatography column provided with an oven, which is then separated into a number of substances. The resultant substances in the form of gas entered the MS section where they are bombarded with the ion source. After ionization, they pass through mass spectrometer where ion separation is achieved by means of electric and magnetic

fields. The mass analyzer is connected with a mass spectrometer which separates elements on the basis of mass/ charge ratios. The detector then detects and converts ionic beams generated from mass analyzer into electric signals. Finally, data is sent to electronics control where it is studied and displayed [65][66]. The schematic diagram of the GC-MS analyzer is shown in Figure 8 [67].
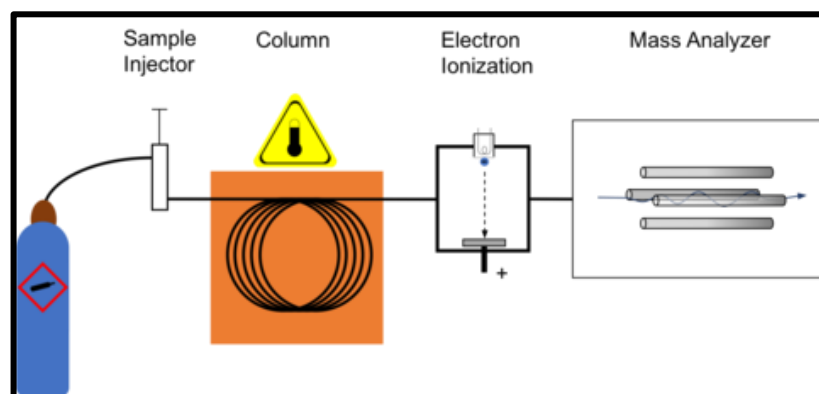

Figure 9. Schematic diagram of GC-MS analyzer

4.6 Temperature programmed desorption (TPD)

For the determination of reaction ability of heterogeneous catalysts, thermo-analytical techniques like TG-DTA, temperature programmed desorption, oxidation and reduction are carried out. They are applied for a better understanding of fluid interaction with active solid catalysts. TPD is an extensively applied technique which evaluates the interaction between reaction gas and solid surface. It characterizes the acidic sites on the surface of the catalyst and gives a better insight of mechanisms (adsorption, desorption, and reactions occurring on the surface) involving in catalytic chemical reactions. It provides useful information regarding desorption rate, desorption kinetic order, adsorption peaks, coverage of surface, desorption energy. This technique is very useful and an excellent choice for characterizing catalysts. It also provides quantitative information related to adsorbed materials via peaks (TCD signals). A number of the peaks depend upon a number of mechanisms involved and the occurrence of different active sites. TPD working principle works on performing the experiment in a reactor where catalysts with active sites features are going to be under study. TPD is a significant feature of catalysis which examines the desorbed molecules which happens when a sample temperature is linearly increasing. During the experimental run, the calculated amount of sample is placed in a sample holder of

a tube reactor which is heated by an oven. The catalyst is then exposed to an inert gas (argon, helium, nitrogen). Ammonia and carbon dioxide can be used. A detector is placed in a reactor which will observe the change in downward gas flow. On the surface of the catalyst, gas is adsorbed which is mostly done by injecting adsorbate into the carrier gas. Heating the catalyst will result in a linear increase in temperature with the passage of time after flushing the un-adsorbed gas. Finally, the adsorbate is desorbing (desorption rate increases) as the temperature of the solid catalyst is increasing which is then observed by a detector (TCD, FID, or MS) [68]. The experimental set up of TPD analyzer is shown in Figure 9.
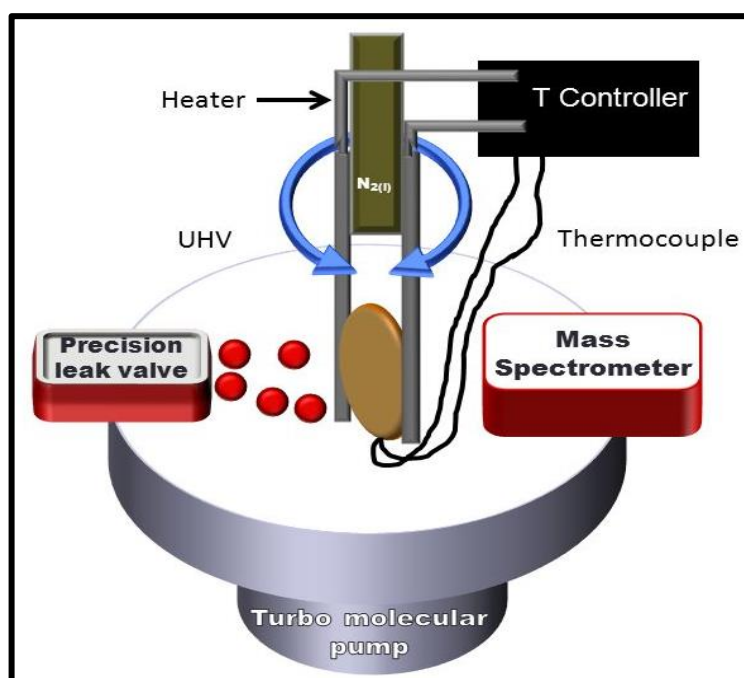

Figure 10. Experimental setup of Temperature programmed desorption analyzer

Chapter 5: Results and Discussion

5.1 Physiochemical characteristics of ZSM-5 catalysts

5.1.1 X-ray Diffraction analysis (XRD)

Figure **11** shows the XRD pattern of a silica sample. It was synthesized by mixing controlled quantities of absolute ethanol, aqueous ammonia, tetraethylorthosilicate, and deionized water at room temperature. The obtained XRD pattern matches up well with the already published data, illustrating that the synthesized silica has a pure phase. The hump at the crystal plane of **111** in the XRD pattern demonstrates the highly amorphous nature of silica [69][70].
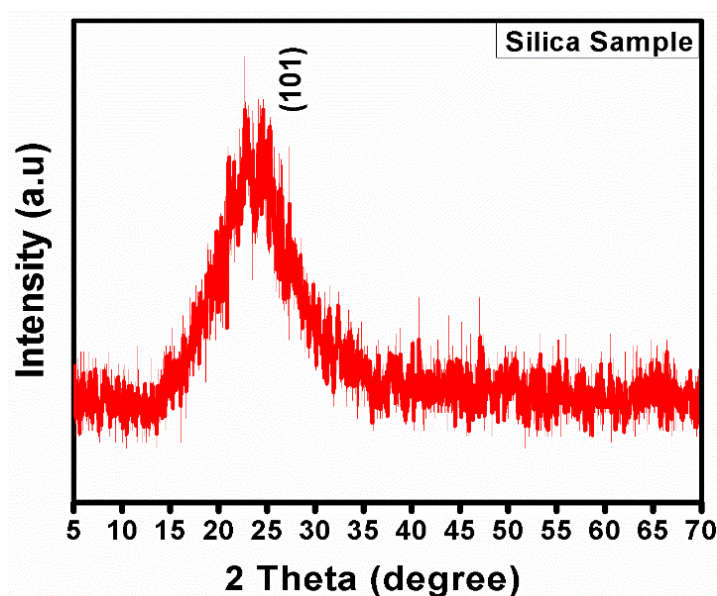

Figure 11. XRD image of silica

Figure **12a-c** shows the XRD pattern of as-synthesized ZSM-5, calcined and ion-exchanged ZSM-5 samples. The obtained diffraction peaks ascribed to ZSM-5 topological structure. The crystal planes of results match well with mordenite framework inverted (MFI) catalog. From the literature, we have studied that the size and crystallinity of ZSM-5 zeolite vary with different ratios of SiO_2/Al_2O_3 ratio. For as-synthesized Sample A, the higher intensity peaks were obtained at 21.82, 28.24, and 36.1, corresponding to the crystal planes of 111, 310, and 200, respectively. After calcination template is decomposed so diffraction peak related to TPABr disappeared. The crystallographic structure was not changed after the

ion-exchanging process. There is no evidence for the presence of new peaks which implied that there is no noticeable information about the new phase. It is already proved in the literature that ion-exchanging does not affect the pure phase of zeolites [45][71][72][73].Figure **12d-e** shows the XRD pattern of calcined ZSM-5 sample B and C. The obtained XRD pattern matches up well with the already published data, illustrating that the synthesized sample is highly crystalline. The diffraction peaks from 10 up to 36° are ascribed to the ZSM-5 zeolite [71].
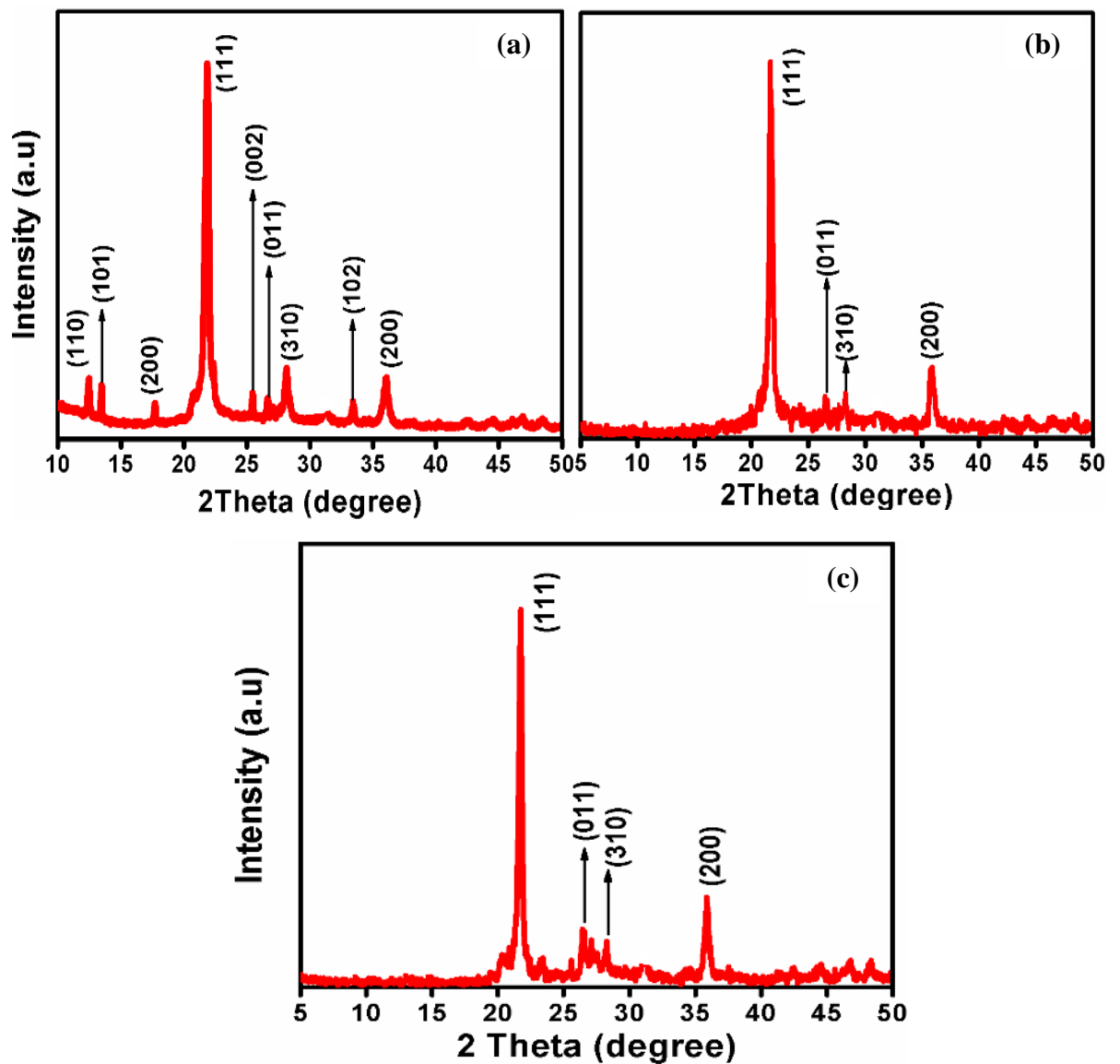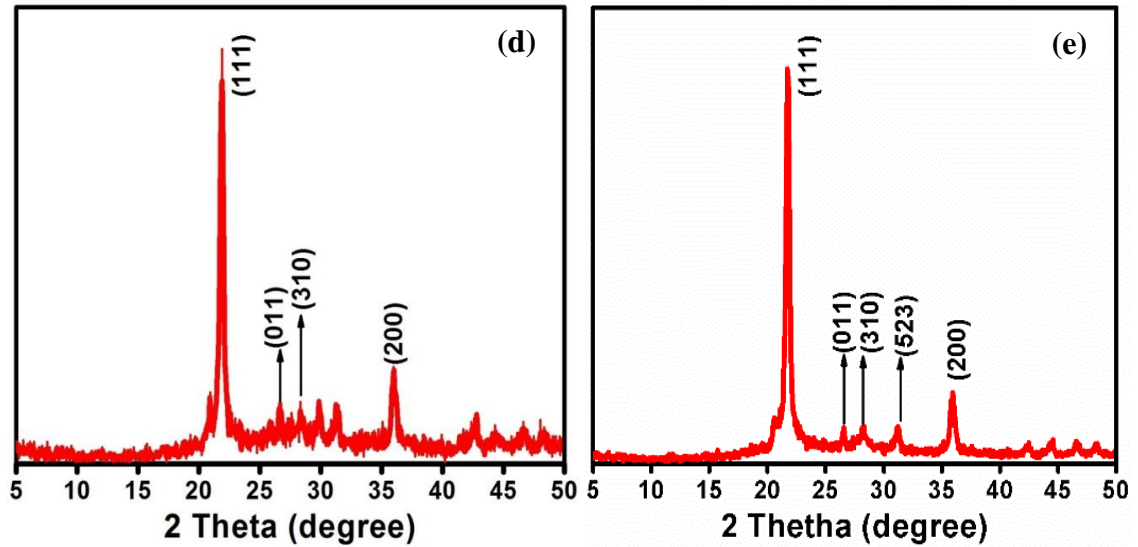
Figure 12. XRD images of ZSM-5 samples **(a)** as-synthesized ZSM-5 Sample A **(b)** Calcined ZSM-5 Sample A **(c)** Ion-exchanged ZSM-5 Sample A **(d)** Calcined ZSM-5 Sample B **(e)** Calcined ZSM-5 Sample C

5.1.2 Scanning electron microscope analysis (SEM)

Figure **13** shows the SEM image of nano silica sample where its spherical morphology with an average diameter of about 228.1 nm is quite noticeable. Silica nanoparticles are in a compact form which can easily be seen in an image [74][75][76].
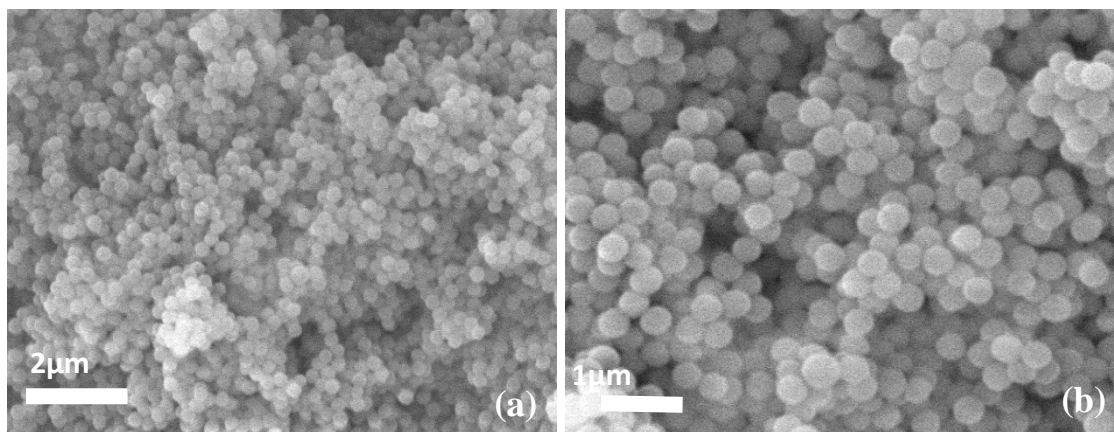

Figure 13. SEM images of silica sample

The silica sample is prepared with a large amount of water and a very small amount of ammonia. For particle formation, mechanism applied is as follow. Firstly during an induction phase, primary particles are converted into stable particles via

35

aggregation. After this initial induction phase, generation of any other primary particles under supersaturation results in the consumption for the expansion of stable particles. The yield of this phase is spherical in morphology and highly monodispersed in size. During an induction phase, the initial level of supersaturation is very important for the determination of particle size. The higher formation of particle size with higher supersaturation rate results in a product with a smaller particle size [52]. After doing a series of experiment, it is observed that the silica particle size increase with an increase in TEOS concentration. Increase in TEOS concentration causes a faster rate of hydrolysis and condensation. TEOS addition is good for the initial supersaturation which in turn results in the production of a large number of stable particles. It also minimizes the time period for the nucleation phase [77].
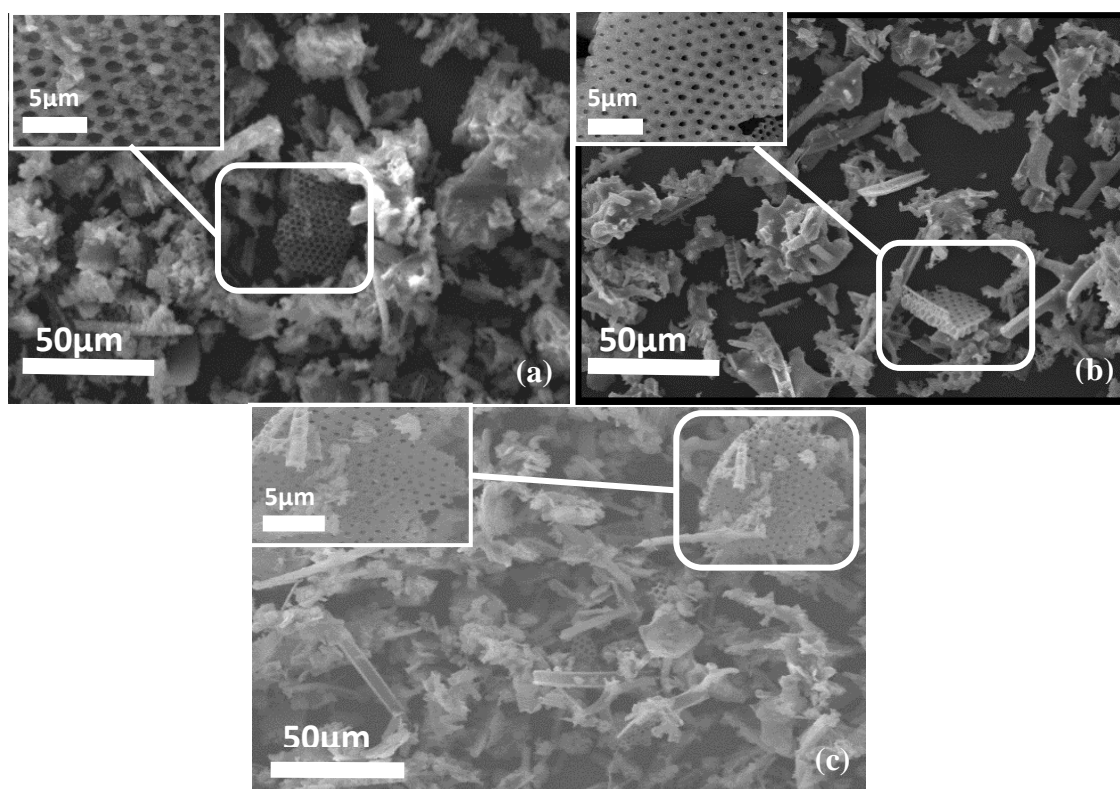

Figure 14. SEM images of calcined ZSM-5 samples **(a)** ZSM-5 sample A **(b)** ZSM-5 sample B **(c)** ZSM-5 sample C

The SEM images of three different calcined samples with varying Si/Al ratios are shown in Figure **14 (a-c)**. The SEM images are showing the aggregates of bulk particles. Among aggregates, the honeycombed structure can be seen. At higher

magnification, a large number of pores in a framework can be observed. These honeycombed structures are scattered in random orientation so we can't see all of them clearly. For these SEM results, nucleation/growth/aggregation mechanism is applied. Tetrapropylammonium bromide/Tetrapropylammonium hydroxide is used as a structural directing agent. The as-synthesized sample contains Na+ and TPA+ ions in its pores and its structure. TPA+ cations act as growth moderator for mesoporous. Precursor species initially nucleate and developed under TPA+ cations and aluminum complexes protection. For nanocrystals, they show stronger affinity and during crystallization nanoparticles become close together within the framework. Due to the high activity of TPA+ cations, nanoparticles gathered together and aggregates comprised of nanoparticles appear in small size i.e. in the form of honeycombed structure. TPA+ cations present a strong affinity towards nanocrystals and nanoparticles can be occluded within the zeolite framework during crystallization. Crystallization time and temperature also affected the crystallinity of samples. During the synthesis of ZSM-5 samples, the crystallization temperature was about 120-170°C for 20-48 hours. In the case of increased synthesis time, larger particles, higher growth rate occurs and have a positive impact on crystallinity. Si/Al ratios are very important regarding the acidity of zeolites irrespective of their sizes. Silica to alumina ratios of different calcined samples are given in Table 2. If these ratios increase, it means numbers of acidic sites decrease [45][53][78][79][80].

Table 2. Silica/ Alumina ratios of different calcined samples

Samples	Si/Al ratios
Calcined ZSM-5 Sample A	24.73
Calcined ZSM-5 Sample B	28.53
Calcined ZSM-5 Sample C	45.63

Figure **15 (a-c)** shows the SEM results of ion-exchanged ZSM-5 samples. There is a drastic change in morphology of sample after ion-exchanging as pores become less clear. After synthesis, ZSM-5 is obtained in Na form (Na-ZSM-5). After ion exchanging with NH_4Cl/NH_4NO_3, the product obtained is in the H^+ form. The H+ increases the number of acidic sites while NH_3 desorbed. After ion-exchanging, their acidity increases. The zeolite's acidity is related to the Lewis and Brønsted acidic sites, which contributes to the total acidity of the zeolite structure. The Lewis acidic sites are related with extra-framework Al_2O_3 species while the Brønsted acidic sites are associated with hydroxyl acidic groups which are connecting the aluminium framework in the zeolite structure. Ion-exchanging with NH_4Cl results in a sharp decrease in Na content and increase in acidic sites (both weak and strong). NH_4Cl is inorganic neutral ammonium salt but its solution is slightly acidic. In this case decrease in Si/Al is very low as compared to strong inorganic ammonium solution (NH_4NO_3), which results in minimal change in acidity of the structure. Inorganic solutions are much active over the dissolution of Si and it is not very controllable. After ion-exchanging, the decrease in porosity of the samples is very prominent as the Si/Al ratio decreases. Mostly siliceous zeolites show stability towards acidic solutions, but they are generally treated with mild acidic solutions to avoid damaging of zeolitic structure. From 3rd SEM result, we deducted that pores are present, but they are clogged [78][81]. From the ion-exchanged SEM images, it is quite difficult to determine the mean size of primary particles [53][81].
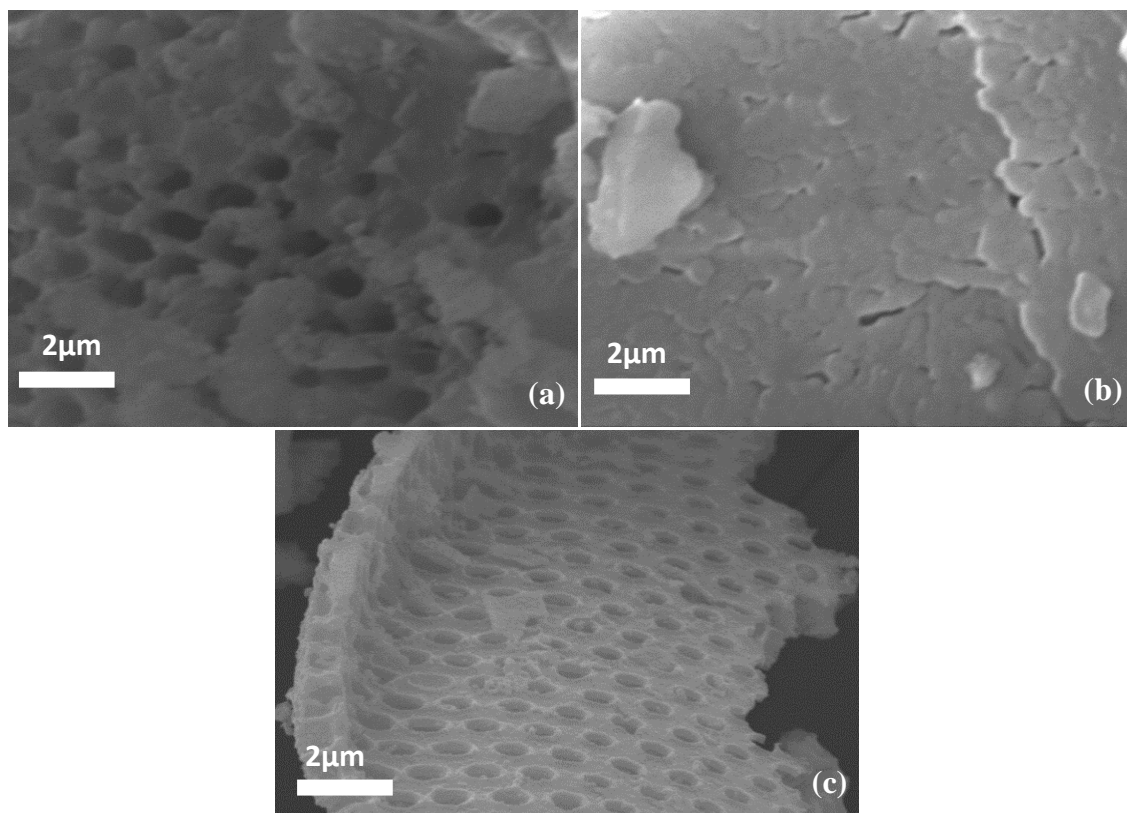
Figure 15. SEM images of ion-exchanged ZSM-5 samples **(a)** ZSM-5 sample A **(b)** ZSM-5 sample B **(c)** ZSM-5 sample C

5.1.3 Fourier-transform infrared spectroscopy (FTIR)

Figure **(16a)** shows the FTIR spectrum of calcined sample A. The broad band at 3398.78 cm^{-1} is ascribed to stretching vibrations of Si-OH group (framework of hydroxyl groups, O-H stretch) and the sharp peak at 1630.12 cm^{-1} is attributed to vibrational stretching (H-O-H stretch) of physically adsorbed water. The peaks at 1084.06 cm^{-1} and 792.29 cm^{-1} are associated with asymmetric and symmetric vibrational stretching of T–O–T (T = Si or Al) tetrahedral bridges (C-O stretch). The peak at 468.59 cm^{-1} is attributed to Si-O-Si vibrational bending (C-O bend). A characteristic peak at 620.58 cm^{-1} showed C-H bending (terminal alkyne bending). Figure **(16b)** shows the calcined sample B FTIR spectrum. The peaks at 2411.86 cm^{-1} and 1880.82 cm^{-1} represented the alkyne C≡C stretch and C=O stretch. Figure **(16c)** shows the FTIR spectrum related to calcined sample C. A characteristic peak at 1221cm^{-1} is attributed to asymmetric vibrational stretching of T-O bond and is a structure-sensitive IR band of the ZSM-5 zeolite. All the important chemical bonds

and functional groups are present in all calcined samples which implies that pure phase is synthesized [6][45][79][80][82].
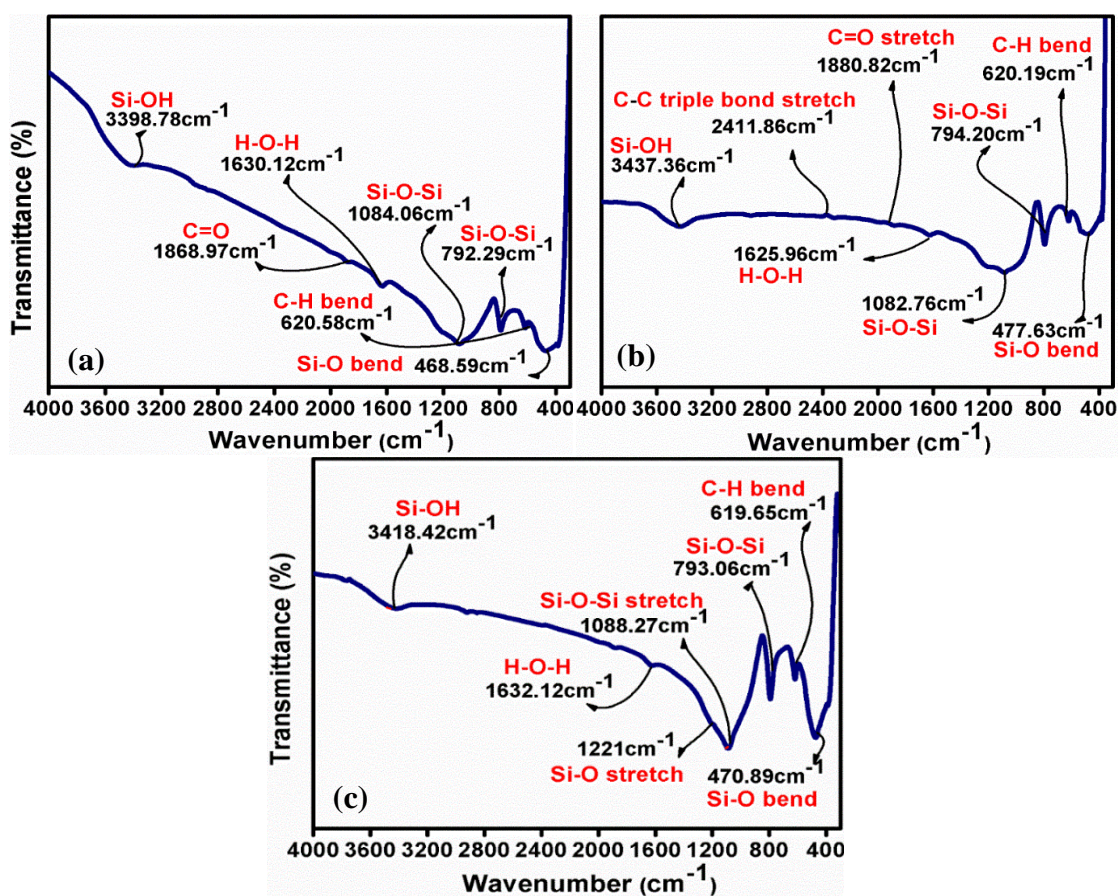

Figure 16. FTIR spectra of Calcined ZSM-5 samples **(a)** ZSM-5 SampleA **(b)** ZSM-5 Sample B **(c)** ZSM-5 Sample C

Figure **(17a)** observes the FTIR spectrum of ion-exchanged sample A. The broad band at 3398.78 cm^{-1} is shifted to 3432.26 cm^{-1} and the sharp peak at 1630.12 cm^{-1} is disappeared. The peaks at 1084.06 cm^{-1} and 792.29 cm^{-1}are shifted to 1090.89 cm^{-1} and 793.51 cm^{-1}. The peak at 468.59 cm^{-1} is shifted to 472.52 cm^{-1}. A characteristic peak at 620.58 cm^{-1} showing C-H bending is shifted to 619.61 cm^{-1}. A characteristic peak at 1868.97 cm^{-1} is disappeared while a new peak at 2418.99 cm^{-1} attributed to C-H stretch appears [45][82][6]. Figure **(17b)** explains the ion-exchanged FTIR spectrum of ion-exchanged sample B. The broad band at 3437.36 cm^{-1} is ascribed to stretching vibrations of Si-OH group is shifted to 3434.49 cm$^{−1}$. After ion-exchanging, all the bonds are shifted and vibrational bands become sharper. While the peaks at 2411.86 cm^{-1} and 1880.82 cm^{-1} disappeared. A characteristic peak at 1223.87 cm^{-1}is a structure-

sensitive IR band of the ZSM-5 zeolite and is attributed to asymmetric vibrational stretching of T-O bond (T= Si, Al) [6][82].Figure **(15c)** reports the ion-exchanged sample C spectrum. The broad band at 3418.42 cm^{-1} ascribed to stretching vibrations of Si-OH group is shifted to 3426.74 cm^{-1}. A characteristic peak at 1221cm^{-1} is disappeared [6][6, 82]. After ion-exchanging, the peaks in the region of 2400-3300cm^{-1} mostly disappear or become weak but it does not result in destabilization of ZSM-5 zeolite structure [73][83].

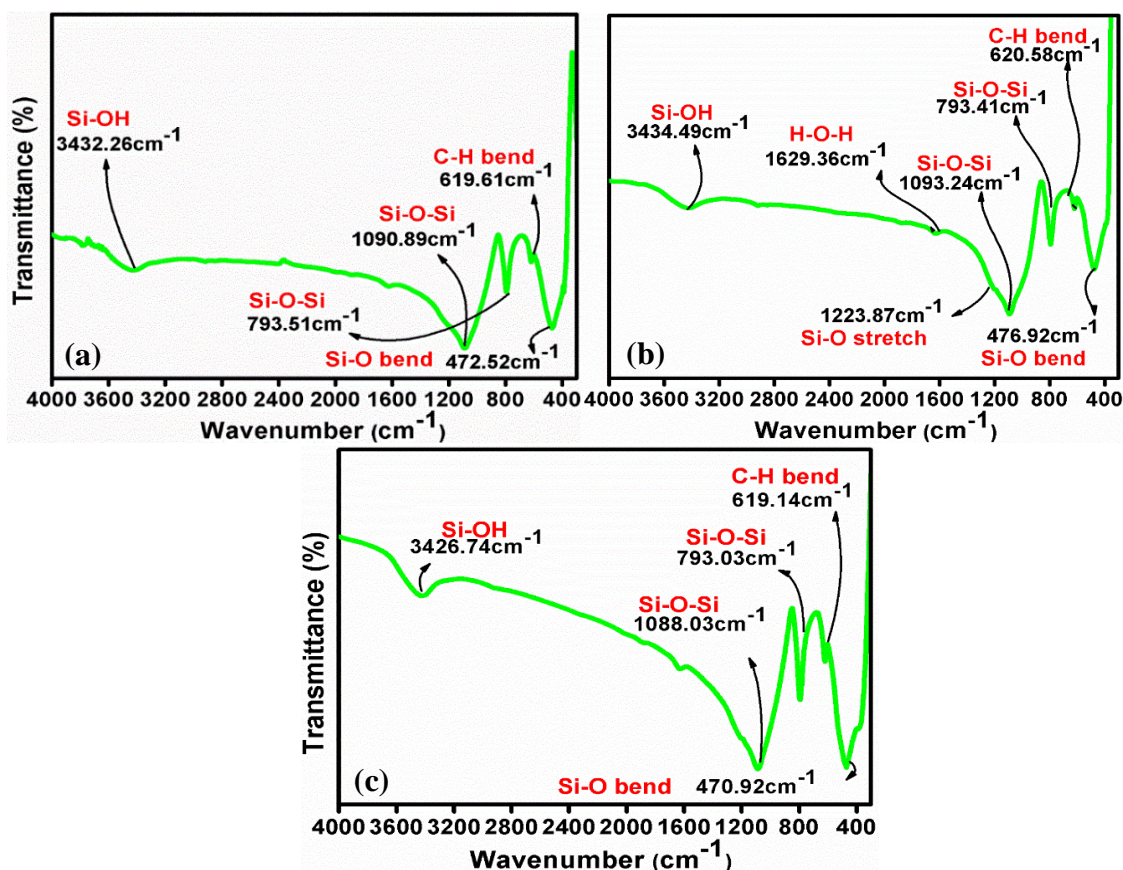**Figure 17.** FTIR spectra of Ion exchanged ZSM-5 samples **(a)** ZSM-5 Sample A **(b)** ZSM-5 Sample B **(c)** ZSM-5 Sample

5.1.4 Differential thermogravimetric analyzer (TG-DTA)

The TG/DTA curves of ZSM-5 Sample B are shown in Figure 14. In Figure **18a**, the DTA curve of calcined ZSM-5 sample A shows an increasing pattern. At a temperature of about 358°C, a broad shows an exothermic peak which corresponds to the stabilization of sample up to 900°C. No other peaks are visible which shows the phase transformation or deformation [79][84]. While the TGA curve of calcined ZSM-5 sample A shows a decreasing pattern describing the total mass loss of water

41

content which is equal to 0.266mg. At 100°C, the removal of water bounded loosely or water entrapped in inner pores of zeolite occur [79]. In Figure **18b**, TG-DTA curve of ion-exchanged ZSM-5 sample A is also showing the increasing pattern. Its pattern is the same as the calcined sample pattern except that humidity loss is about 0.338mg by TG curve. The exothermic peak is obtained at 389°C. DTA curves also indicate that ion-exchanged ZSM-5 zeolite is stable up to 900°C. The acidity of both samples is quite different. HZSM-5 is more acidic than calcined ZSM-5 but there is no different in their TFG-DTA curves [79][84].
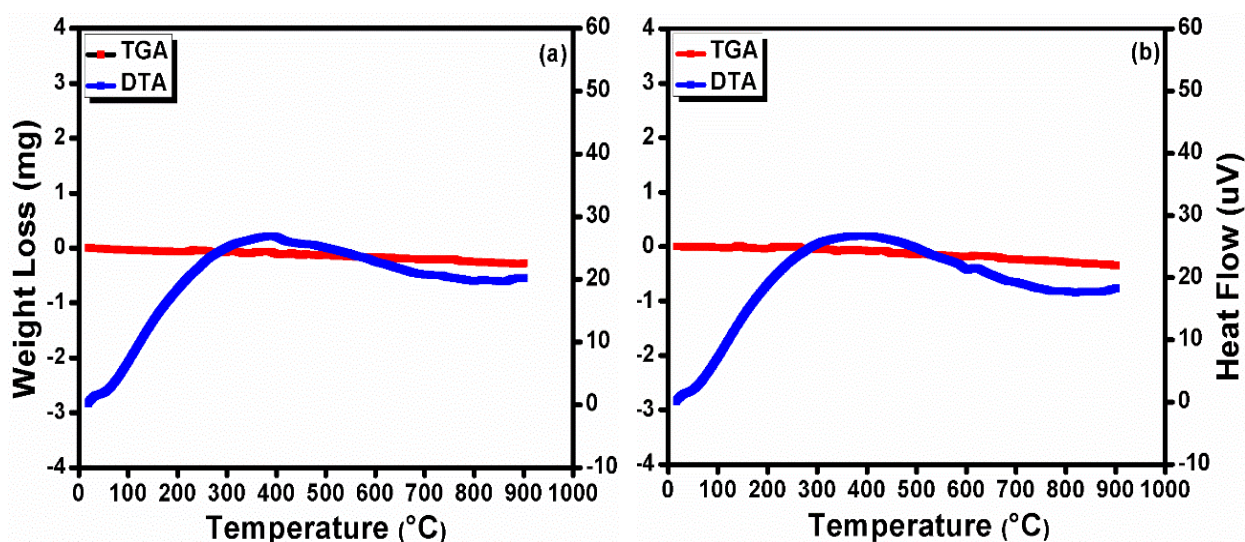

Figure 18. TG/DTA curves of ZSM-5 samples **(a)** Calcined ZSM-5

(b) Ion-exchanged ZSM-5

5.1.5 Temperature programmed desorption (TPD)

TPD analysis is done to determine the acidity of zeolite catalysts. Figure **19** shows the NH$_3$-TPD profiles of un-calcined, calcined and ion-exchanged ZSM-5 samples. For TPD analysis, Helium (He) was used as a carrier gas. The calculated amount of catalyst was placed in the sample holder, where it was heated by an oven. Before the experimental run, the catalyst was degassed by helium for 1 hour at 450-550°C. During the experiment, the catalyst was exposed to the mixture of He and ammonia (NH$_3$). After feeding the mixture with a flow rate of 17.03g/mol, the temperature of the mixture was increased to 800°C. After exposure, ammonia was adsorbed on the surface of the catalyst. But when the temperature of catalyst increases, gas adsorbed will start desorbing which is shown by desorption peaks. Figure **19a** showing two

clear peaks with small additional peaks. The peaks around 230°C and 395°C ascribed to weak and strong acidic sites. The peak at 230°C is not very intense, it means desorption rate is low and it is also attributed to chemisorption of NH_3 on weak acidic sites. The rate of desorption increase with an increase in the temperature of the sample shown by a peak at 395°C. This peak corresponds to desorption of NH_3 on Bronsted acidic sites. The Si/Al ratio greatly affects the intensity of peaks. Due to the low availability of aluminum exchanging sites (high Si/Al ratio), the peaks show low acidic sites density. The additional peaks determine that more than one mechanism (adsorption, desorption or surface reaction) are occurring or different binding sites are available. In Figure **19b**, the intensity of both low (295°C) and high temperature (490°C) peak increase after calcination treatment in comparison to uncalcined sample and shifted towards high temperature due to enhancement in zeolite framework stability and availability of active sites. After ion-exchanging, the sample (H-ZSM-5) is showing two clear broad desorption peaks in Figure **19c.** The desorption rate is higher at 600 °C than at 300°C. The peaks are related to desorption of NH_3 from weak (low-temperature peak) and strong (high-temperature peak) acidic sites. After ion-exchanging desorption rates of both peaks also increases. At high temperature, ammonia desorption peak is assigned to Bronsted acidic sites while at low temperature (300°C), the peak is ascribed to physically adsorbed ammonia /weak ammonia adsorption (non-acidic hydroxyl group) to the zeolite framework. The peak area determines the number of acidic sites. As it is shown by TPD profiles, HZSM-5 has the highest acidity in comparison to uncalcined and calcined samples. The acidity of uncalcined and calcined samples is related to Lewis acidic sites. While ion-exchanged ZSM-5 sample has Bronsted acidic sites which are much stronger in zeolite than Lewis acidic sites. The catalytic activity of ZSM-5 is because of this acidity. When the acidity of zeolites exceeds the certain limit, it will result in a decrease of porosity which in turn will affect the catalytic activity of the catalyst. Highly acidic nature of zeolites also threatens the generation of coke [35][85][86][87].
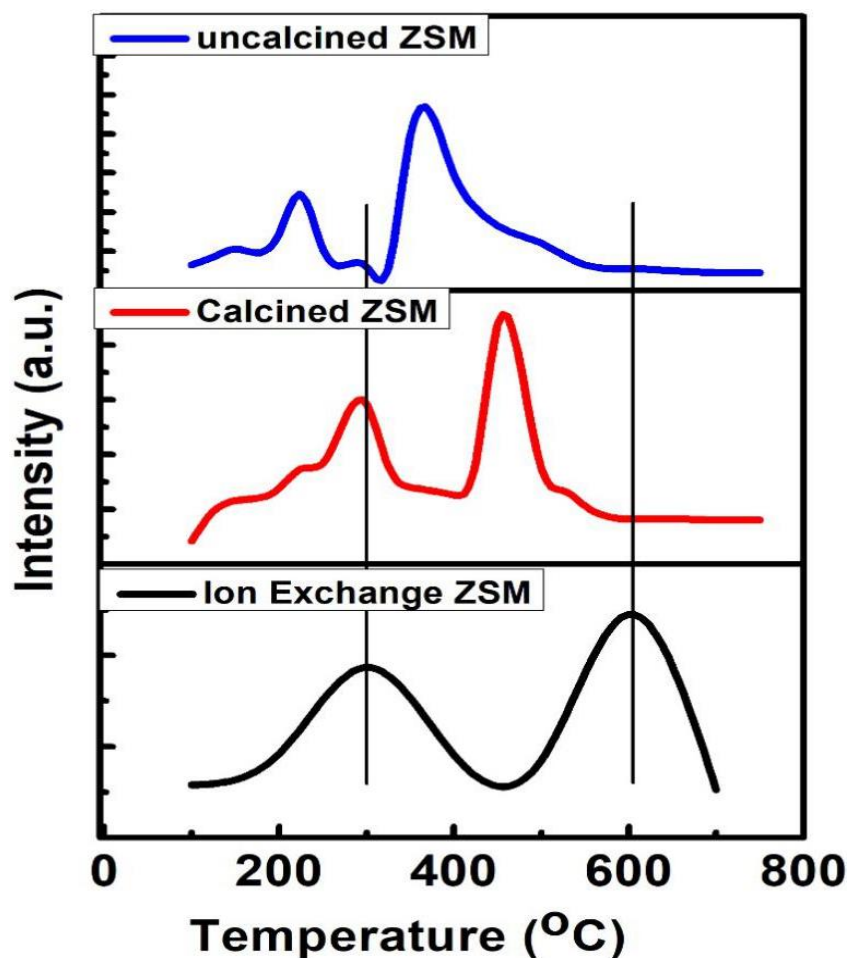
Figure 19. TPD profiles of ZSM-5 samples **a.** Un-calcined **b.** Calcined **c.** ion-exchanged

5.2 Kinetic study of n-hexane catalytic cracking

5.2.1 Reaction Mechanism

According to the literature, there are two mechanisms (unimolecular and bimolecular) involved in the catalytic cracking of n-hexane over ZSM-5. The main pathway used for paraffin (n-hexane) cracking is a unimolecular mechanism. In this study, the proposed reaction mechanism involves the following steps.

- The protonation of ZSM-5 over the C-C or C-H bonds of n-hexane which results in the formation of pentacoordianted carbonium ion on Bronsted acidic sites.

- This adsorbed carbonium ion is high energy transition state which is further cracked to the lower alkanes (methane, ethane, propane, and butane), alkenes (ethylene, propylene, and butadienes) and hydrogen yield.

For n-hexane catalytic cracking at higher temperatures, the unimolecular mechanism is preferred over bimolecular one. The bimolecular cracking is not a favorable pathway for enhancing the manufacturing of olefins, which leads the hydrogen transfer reaction, where the olefin hydrogenation rate is prominent than paraffin dehydrogenation rate [13][88][89].
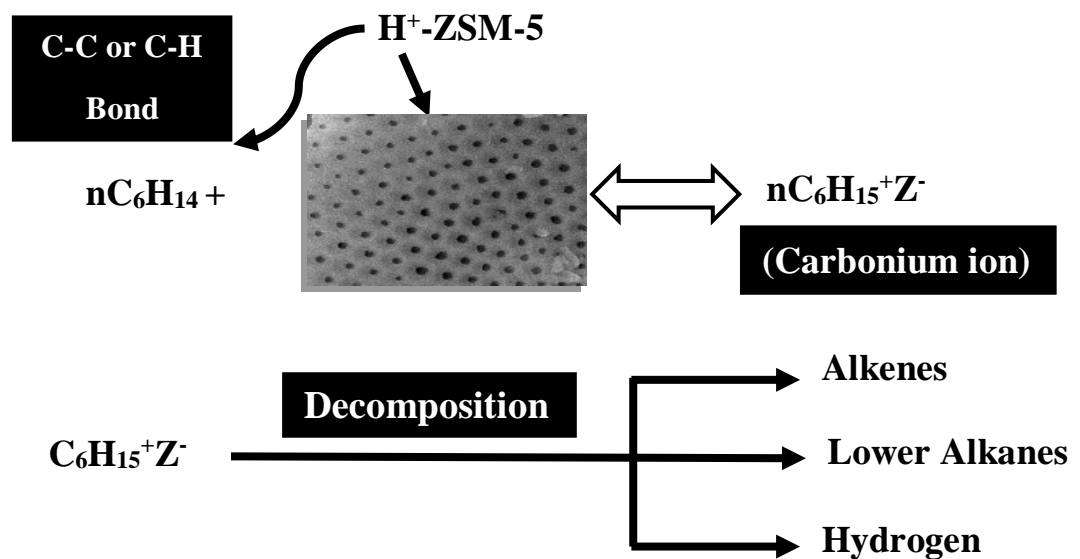

Figure 20. Schematic diagram of reaction mechanism of n-hexane

5.2.2 Kinetic study

In order to determine the n-hexane catalytic cracking results, the kinetic analysis is done. The catalytic reaction was done in a microreactor-Packed bed reactor (PBR) containing a porous catalyst. The performance equation of which is;

$$\frac{W}{F_{Ao}} = \int_0^{X_A} \frac{dX_A}{-r_A} \tag{3}$$

As the flow path of the reactor is very narrow, we assumed that the rate of reaction is average. For given reaction conditions in a microreactor-PBR, the performance equation of differential reactor is applied to determine the order of the reaction.

$$\frac{W}{F_{Ao}} = \int_0^{XA} \frac{dXA}{-rAavg} \tag{4}$$

$$\frac{W}{F_{Ao}} = \frac{1}{-rAavg} \int_0^{XA} dXA \tag{5}$$

$$\frac{W}{F_{Ao}} = \frac{XA-0}{-rAavg} \tag{6}$$

$$\frac{W}{F_{Ao}} = \frac{XA}{-rAavg} \tag{7}$$

Where W is the weight of catalysts, F_{AO} is the molecular flux, X_A is the conversion of reactants while r_A is the rate of reaction. The initial concentrations of n-hexane are known and final concentration values (C_A) are determined at the outlet of the microreactor. The values of conversion of n-hexane can be determined by initial and final concentrations of n-hexane.

$$X_A = 1 - \frac{CA}{CAo} \tag{8}$$

The values of W, F_{AO}, C_A, and C_{AO} are known, so we can easily determine the rates of reaction of n-hexane. Then the graph (Figure 21) is plotted between r_A and C_{AO} values of n-hexane to determine the order of reaction (n). The slope of the plot is approximately equal to 1. The straight line is obtained which tells that the rate of reaction of n-hexane is proportional to the concentration of n-hexane. The decrease in concentration of n-hexane results in enhanced n-hexane rate of reaction. Catalytic cracking of n-hexane is first order regarding the n-hexane concentrations. The identical concentration dependence on the rate of reaction is determined at reaction temperatures of 500°C and 600°C [90].
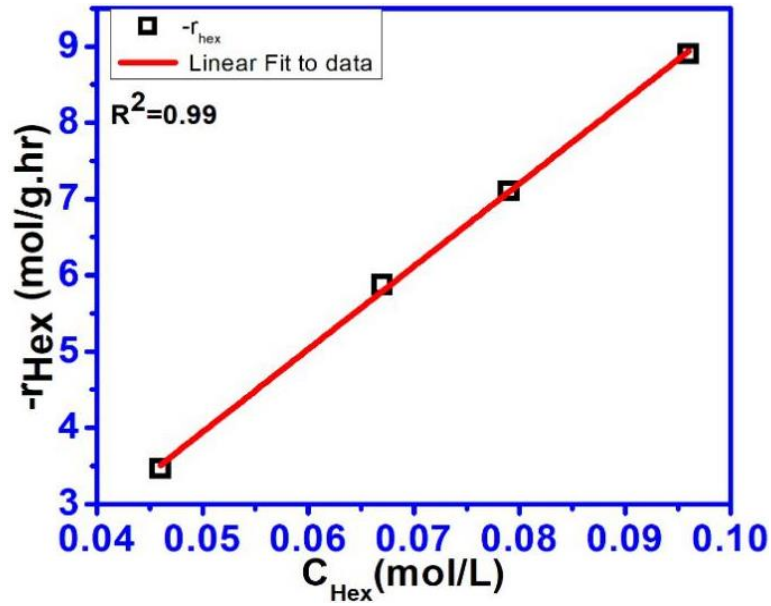
Figure 21. Concentration vs rate of reaction in n-hexane cracking

The equation for the rate of reaction is;

$$-r_A = kC_A{}^n \qquad (9)$$

Replace $kC_A{}^n$ with $-r_A$ in the performance equation of PBR (eq. 3) and value of the order of reaction (n) is equal to 1. The performance equation then becomes;

$$\frac{W}{F_{Ao}} = \int_0^{X_A} \frac{dX_A}{kC_A} \qquad (10)$$

$$\frac{W}{F_{Ao}} = \int_0^{X_A} \frac{dX_A}{kC_{Ao}(1-X_A)} \qquad (11)$$

$$\frac{W}{F_{Ao}} = \frac{1}{kC_{Ao}} \int_0^{X_A} \frac{dX_A}{(1-X_A)} \qquad (12)$$

$$\frac{W}{F_{Ao}} = \frac{-\ln(1-X_A)}{kC_{Ao}} \qquad (13)$$

Where, k is rate constant. The graphs are plotted between W/F_{AO} and $-\ln(1-X_A)/C_{AO}$ at 500°C and 600°C for both calcined and ion-exchanged ZSM-5 samples to determine their catalytic activity in terms of rate constants (K) and activation energy (E_a). The values of W are 20mg, 50mg, 80mg, 110mg, and 140mg. For calcined and ion-exchanged samples, W/F_{AO} is the varying as the value of W varies from 20-140mg. The variation in initial concentrations of n-hexane results in conversion values. The slopes of the obtained curves are equal to 1/k. The values of k for both samples are found by the following equation.

$$n = \frac{1}{k} \qquad (14)$$

From the slopes of these curves at both temperatures for both samples, values of rate constants were determined. For the calcined sample, the rate constants obtained at 500°C and 600°C are 4.49×10^{-4} s^{-1} and 6.63×10^{-4} s^{-1}. While for the ion-exchanged samples, the rate constants acquired at 500°C and 600°C are 3.21×10^{-4} s^{-1} and 5.68×10^{-4} s^{-1}. **Figures 22 and 23** show that with an increase in temperature, the rate constant increases which in turn increases the rate of reaction and conversion of n-hexane over both ZSM-5 samples. At 600°C, catalytic cracking of n-hexane over zeolite catalysts is higher in comparison to 500°C. The reaction rate constants obtained for n-hexane cracking at both 500°C and 600°C are higher in comparison to the ion-exchanged samples. The increase in W values increases the conversion of n-hexane as more active sites are available for the reaction.

To determine the values of activation energy (Ea) for both calcined and ion-exchanged samples, the Arrhenius equation is applied.

$$\text{In}\frac{k2}{k1} = \frac{E}{R} \left(\frac{1}{T1} - \frac{1}{T2} \right) \qquad (15)$$

The activation energy (E) for calcined samples is 21867.99 J/mol which is less than 32018.3 J/mol obtained for ion-exchanged samples. The catalytic activity of calcined samples is quite higher with a higher value of rate constants at both temperatures and lower value of activation energy in comparison to ion-exchanged samples under the same conditions. The acidity of zeolite catalyst plays a vital role in the catalytic cracking of paraffins. The zeolite's acidity is associated with Bronsted and Lewis acidic sites [43]. They affect the conversion and product yield but not the selectivity of products. In comparison to the already published literature on n-hexane catalytic cracking over ZSM-5 catalysts, activation energies obtained are in the range of 123-126×10^3 J/mol while the catalysts prepared in this study have activation energies of 21.867×10^3 J/mol (calcined sample) and 32.018×10^3 J/mol (ion-exchanged samples) [87]. The decay of catalyst is very high with highly acidic zeolites. The E for slow deactivation rate is high for HZSM-5 [91]. ZSM-5 zeolite with high acidic density or strong acidic sites has more chances of carbon/coke deposition which results in pore blockage. Stable and consistent activity occurs with reduced strong acidic sites. High

temperature also lessens the acidity of zeolite catalyst to some extent which leads to lower activity of catalyst [92]
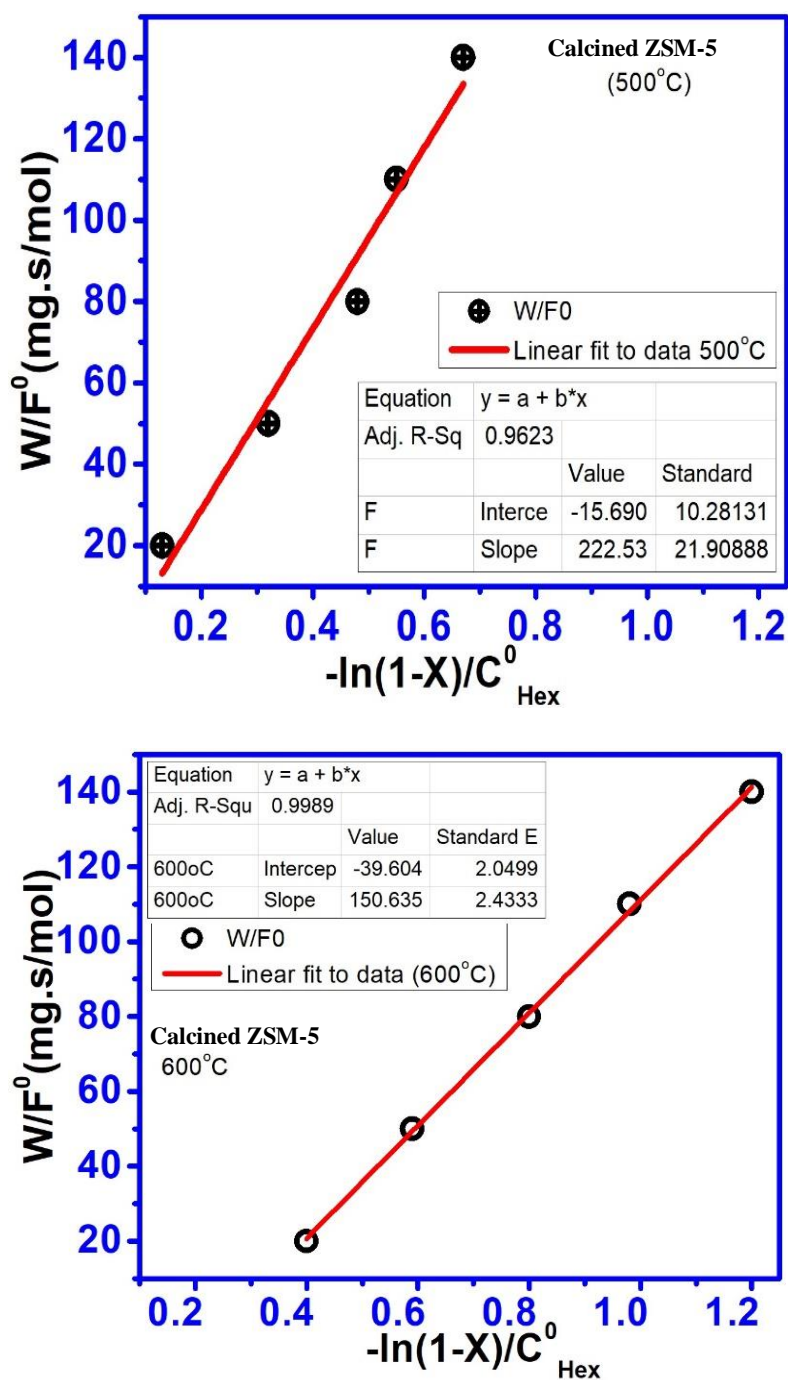
Figure 22. Relationship between W/F_{Ao} and $-In(1-X)/C_{Ao}$ in n-hexane cracking over calcined ZSM-5 zeolite samples at T=500°C and 600°C

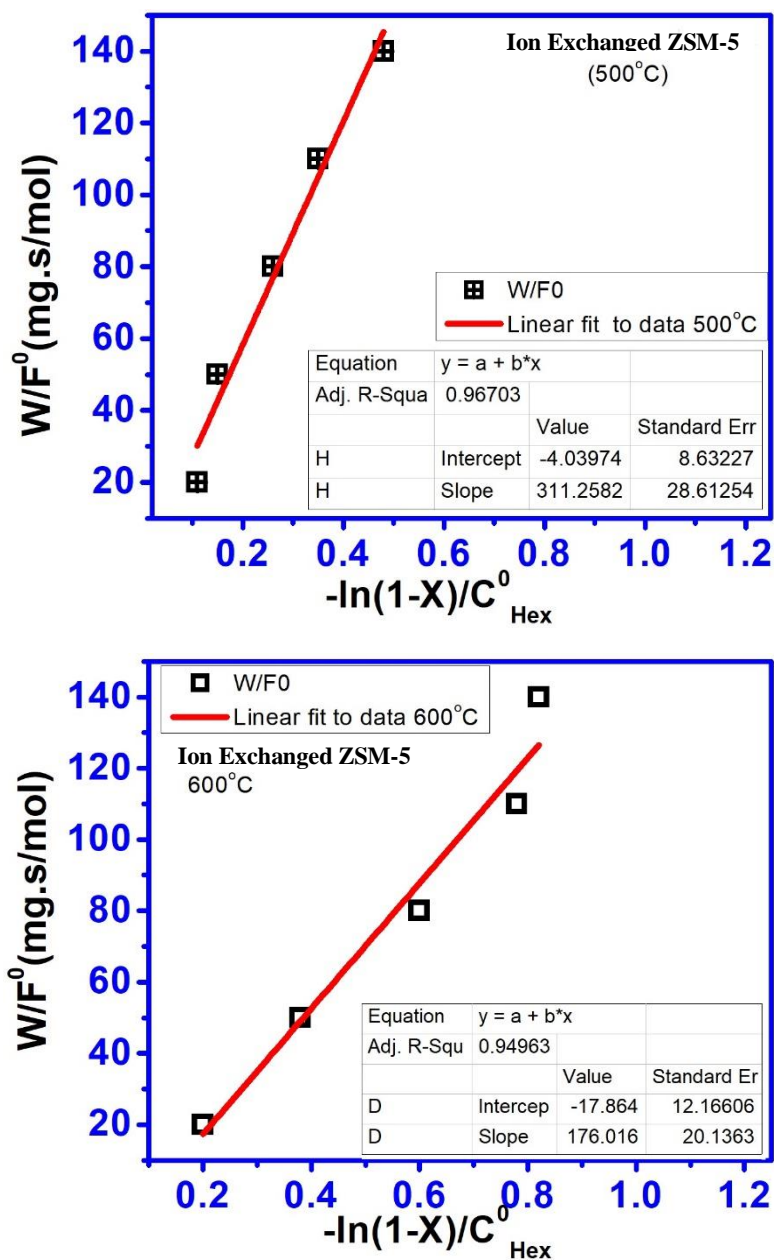**Figure 23.** Relationship between W/F_{Ao} and $-\ln(1-X)/C_{Ao}$ in n-hexane cracking over ion-exchanged ZSM-5 zeolite samples at T=500°C and 600°C

The products generated as a result of n-hexane cracking over both zeolite samples are;

1. Ethylene (C_2H_4)
2. Propylene (C_3H_6)
3. Methane (CH_4)
4. n-Butane (C_4H_{10})

The products obtained are determined by online GC connected with the microreactor.

Conclusion and Recommendations

Conclusion

ZSM-5 zeolite catalysts are synthesized via hydrothermal methods using different structural directing agents. The as-synthesized samples are calcined and then ion-exchanged by using different ammonium precursors (NH_4Cl/NH_4NO_3). The resulted catalysts are characterized by various analytical techniques and successfully applied to the n-hexane conversion at temperatures of about 500°C and 600°C. XRD and TG-DTA results proved that pure phase of ZSM-5 zeolite is synthesized. In this study, the acidity of HZSM-5 is quite higher than calcined samples which are shown by TPD profiles. The high acidity (low Si/Al) results in low porosity as shown in SEM images which in turns affects the activity of the catalyst. The decay of catalyst is very high with highly acidic zeolites. The catalytic activities of calcined and ion-exchanged samples are compared at both temperatures under the same conditions. The results showed that with increasing temperature, calcined samples are showing much better activity than ion-exchanged samples because of their low acidity. Also at the different temperatures, the same sample is showing different activity. The acidity of zeolite catalyst plays a vital role in the catalytic cracking of paraffin. The high temperatures of 500°C and 600°C reduced the acidity which favors the conversion of n-hexane. The rate constants for calcined samples are $4.49{\times}10^{-4}$ (500°C) and $6.63{\times}10^{-4}$ s^{-1} (600°C) while for ion-exchanged samples $3.21{\times}10^{-4}$ s^{-1} (500°C) and $5.68{\times}10^{-4}$ s^{-1} and (600°C) are obtained. In comparison to the already published literature on n-hexane catalytic cracking over ZSM-5 catalysts, activation energies obtained are in the range of $123\text{-}126{\times}10^{3}$ J/mol while the catalysts prepared in this study have activation energies of $21.867{\times}10^{3}$ J/mol (calcined sample) and $32.018 {\times}10^{3}$ J/mol (ion-exchanged samples).

Recommendations

Up till now, Pakistan is lacking naphtha cracker which resulted in a limited yield of petrochemicals. ZSM-5 zeolite catalysts can be applied to naphtha or any other petroleum feeds on a large scale for production of light olefins. The processes used for the synthesis of ZSM-5 are still at the laboratory level so scaling them up to an industrial scale will be economical considering their impact. To study the applications and production of olefins at a large scale is quite beneficial. And also the hydrothermal stability of ion-exchanged ZSM-5 needs to be improved. The acidity of ion-exchanged ZSM-5 needs to be by dealumination or reducing the crystal size.

References

[1]   *50MW wind energy project set up in Thatta*, in *Pakistan Today*. 2012, Staff Report: Pakistan.

[2]   Bhutta, Z., *Power shortfall hits record peak*, in *The Express Tribune*. 2018: Pakistan.

[3]   Vassiliou, M.S., *Historical dictionary of the petroleum industry*. 2018: Rowman & Littlefield.

[4]   Amghizar, I., et al., *New trends in olefin production.* Engineering, 2017. **3**(2): p. 171-178.

[5]   Ren, T., M. Patel, and K. Blok, *Olefins from conventional and heavy feedstocks: Energy use in steam cracking and alternative processes.* Energy, 2006. **31**(4): p. 425-451.

[6]   Wu, T., et al., *Enhanced selectivity of propylene in butylene catalytic cracking over W-ZSM-5.* Fuel Processing Technology, 2018. **173**: p. 143-152.

[7]   Corma, A., et al., *Crude oil to chemicals: light olefins from crude oil.* Catalysis Science & Technology, 2017. **7**(1): p. 12-46.

[8]   Sadrameli, S., *Thermal/catalytic cracking of hydrocarbons for the production of olefins: A state-of-the-art review I: Thermal cracking review.* Fuel, 2015. **140**: p. 102-115.

[9]   Hajheidary, M., M. Ghashghaee, and R. Karimzadeh, *Olefins production from LPG via dehydrogenative cracking over three ZSM-5 catalysts.* Journal of scientific and industrial research, 2013. **72**(12): p. 760-766.

[10]   Akah, A., *Application of rare earths in fluid catalytic cracking: A review.* Journal of Rare Earths, 2017. **35**(10): p. 941-956.

[11]   Siddiqui, M.B., et al., *Enhancing the production of light olefins by catalytic cracking of FCC naphtha over mesoporous ZSM-5 catalyst.* Topics in Catalysis, 2010. **53**(19-20): p. 1387-1393.

[12]   Vogt, E. and B. Weckhuysen, *Fluid catalytic cracking: recent developments on the grand old lady of zeolite catalysis.* Chemical Society Reviews, 2015. **44**(20): p. 7342-7370.

[13]   Alipour, S.M., *Recent advances in naphtha catalytic cracking by nano ZSM-5: A review.* Chinese Journal of Catalysis, 2016. **37**(5): p. 671-680.

[14]   Aitani, A., T. Yoshikawa, and T. Ino, *Maximization of FCC light olefins by high severity operation and ZSM-5 addition.* Catalysis Today, 2000. **60**(1-2): p. 111-117.

[15]   Primo, A. and H. Garcia, *Zeolites as catalysts in oil refining.* Chemical Society Reviews, 2014. **43**(22): p. 7548-7561.

[16]   Yoshimura, Y., et al., *Catalytic cracking of naphtha to light olefins.* Catalysis Surveys from Japan, 2001. **4**(2): p. 157-167.

[17]   Sadrameli, S., *Thermal/catalytic cracking of liquid hydrocarbons for the production of olefins: A state-of-the-art review II: Catalytic cracking review.* Fuel, 2016. **173**: p. 285-297.

[18]   Mukhopadhyay, R. and D. Kunzru, *Catalytic pyrolysis of naphtha on calcium aluminate catalysts. Effect of potassium carbonate impregnation.* Industrial & engineering chemistry research, 1993. **32**(9): p. 1914-1920.

[19]   Jeong, S.M., J.H. Chae, and W.-H. Lee, *Study on the catalytic pyrolysis of naphtha over a KVO$_3$/α-Al$_2$O$_3$ catalyst for production of light olefins.* Industrial & engineering chemistry research, 2001. **40**(26): p. 6081-6086.

[20]   Song, J.H., et al., *Catalytic cracking of n-hexane over MoO$_2$.* Journal of Molecular Catalysis A: Chemical, 2002. **184**(1-2): p. 197-202.

[21]   Pant, K. and D. Kunzru, *Catalytic pyrolysis of n-heptane on unpromoted and potassium promoted calcium aluminates.* Chemical Engineering Journal, 2002. **87**(2): p. 219-225.

[22]   Rodriguez-Reinoso, F., *The role of carbon materials in heterogeneous catalysis.* Carbon, 1998. **36**(3): p. 159-175.

[23]   Fischer, J.E. and A.T. Johnson, *Electronic properties of carbon nanotubes.* Current opinion in solid state & materials science, 1999. **1**(4): p. 28-33.

[24]   Grobert, N., et al., *Processing, characterisation and theory of carbon nanotubes containing SiOx-based nanocomposites.* Journal of Ceramic Processing Research, 2003. **4**(1): p. 1-5.

[25]   Wang, Y., et al., *Microstructure and thermal characteristic of Si-coated multi-walled carbon nanotubes.* Nanotechnology, 2006. **17**(15): p. 3817.

[26]   Fu, Q., C. Lu, and J. Liu, *Selective coating of single wall carbon nanotubes with thin SiO2 layer.* Nano Letters, 2002. **2**(4): p. 329-332.

[27]   Keyvanloo, K., et al., *Investigating the effect of key factors, their interactions and optimization of naphtha steam cracking by statistical design of experiments.* Journal of Analytical and Applied Pyrolysis, 2010. **87**(2): p. 224-230.

[28]   Sheibani, S., *Catalyst synthesis over MWNTs for light olefin production.* 2012, University of Tarbiat Modares: Tehran, Iran.

[29]   Keyvanloo, K., *Experimental studies on thermal catalytic cracking of naphtha over carbon nanotubes modified with rare earth elements for production of light olefins*. 2010, University of Tarbiat Modares: Tehran, Iran.

[30]   Zhao, G.-L., et al., *Catalytic cracking reactions of C4-olefin over zeolites H-ZSM-5, H-mordenite and H-SAPO-34*, in *Studies in Surface Science and Catalysis*. 2007, Elsevier. p. 1307-1312.

[31]   Zhu, X., et al., *Catalytic cracking of C4 alkenes to propene and ethene: Influences of zeolites pore structures and Si/Al2 ratios.* Applied Catalysis A: General, 2005. **288**(1-2): p. 134-142.

[32]   Lee, S.-H., et al., *Synthesis, characterization, and catalytic properties of zeolites IM-5 and NU-88.* Journal of Catalysis, 2003. **215**(1): p. 151-170.

[33]   Blay, V., et al., *Engineering zeolites for catalytic cracking to light olefins.* ACS Catalysis, 2017. **7**(10): p. 6542-6566.

[34]   Rahimi, N. and R. Karimzadeh, *Catalytic cracking of hydrocarbons over modified ZSM-5 zeolites to produce light olefins: A review.* Applied Catalysis A: General, 2011. **398**(1-2): p. 1-17.

[35]   Al-Shammari, A.A., et al., *Catalytic cracking of heavy naphtha-range hydrocarbons over different zeolites structures.* Fuel Processing Technology, 2014. **122**: p. 12-22.

[36]   Kumar, J., R. Jha, and B.K. Modhera, *Applications of Zeolite with Additives in Petroleum Refinery.* International Journal of Chemistry and Chemical Engineering, 2013. **3**(2): p. 75-80.

[37]   Abrevaya, H. *From Zeolites to Porous MOF Materials.* In *the 40th Anniversary of International Zeolite Conference.* 2007. Beijing, China.

[38]   Cubillos Lobo, J.A. and W.F. Hölderich, *Heterogeneous asymmetric epoxidation of cis-ethyl cinnamte over Jacobsen's catalyst immobilized in inorganic porous materials.* 2005, Fakultät für Mathematik, Informatik und Naturwissenschaften.

[39]   Soni, D., et al., *Catalytic cracking process enhances production of olefins.* Petroleum technology quarterly, 2009. **14**(5).

[40]   Corma, A., et al., *IM-5: A highly thermal and hydrothermal shape-selective cracking zeolite.* Journal of Catalysis, 2002. **206**(1): p. 125-133.

[41]   Kubů, M., S.I. Zones, and J. Čejka, *TUN, IMF and-SVR Zeolites; Synthesis, Properties and Acidity.* Topics in Catalysis, 2010. **53**(19-20): p. 1330-1339.

[42]   Al Naimi, E.I. and A.A. Garforth, *The effect of zeolite structure and pore systems on maximizing propylene production in FCC unit.* Chemical engineering, 2015. **43**.

[43]   Konno, H., et al., *Effectiveness of nano-scale ZSM-5 zeolite and its deactivation mechanism on catalytic cracking of representative hydrocarbons of naphtha.* Microporous and Mesoporous Materials, 2013. **175**: p. 25-33.

[44]   Konno, H., et al., *Kinetics of the catalytic cracking of naphtha over ZSM-5 zeolite: effect of reduced crystal size on the reaction of naphthenes.* Catalysis science & technology, 2014. **4**(12): p. 4265-4273.

[45]   Li, Y., et al., *Synthesis of ZSM-5 zeolite from diatomite for fluid catalytic cracking (FCC) application.* Applied Petrochemical Research, 2015. **5**(4): p. 347-353.

[46]   Ji, Y., et al., *Phosphorus modification increases catalytic activity and stability of ZSM-5 zeolite on supercritical catalytic cracking of n-dodecane.* Journal of Solid State Chemistry, 2017. **251**: p. 7-13.

[47]   Zhao, Y., et al., *Enhancing hydrothermal stability of nano-sized HZSM-5 zeolite by phosphorus modification for olefin catalytic cracking of full-range FCC gasoline.* Chinese Journal of Catalysis, 2017. **38**(1): p. 138-145.

[48]   Hou, X., et al., *Effects of regeneration of ZSM-5 based catalysts on light olefins production in n-pentane catalytic cracking.* Chemical Engineering Journal, 2017. **321**: p. 572-583.

[49]   Widayat, W. and A. Annisa. *Synthesis and Characterization of ZSM-5 Catalyst at Different Temperatures.* In *IOP Conference Series: Materials Science and Engineering.* 2017. IOP Publishing.

[50]   ZHONGNENG, L.S.W.D.L., 12, *Method for preparing nano zsm-5 zeolite by using diatomaceous earth.* 2014, China Petroleum and Chemical Corporation: China. p. 12.

[51]   Müller, M., G. Harvey, and R. Prins, *Comparison of the dealumination of zeolites beta, mordenite, ZSM-5 and ferrierite by thermal treatment, leaching with oxalic acid and treatment with SiCl4 by 1H, 29Si and 27Al MAS NMR.* Microporous and mesoporous materials, 2000. **34**(2): p. 135-147.

[52]   Ibrahim, I.A., A. Zikry, and M.A. Sharaf, *Preparation of spherical silica nanoparticles: Stober silica.* J. Am. Sci, 2010. **6**(11): p. 985-989.

[53]   Li, H., et al., *Direct synthesis of high-silica nano ZSM-5 aggregates with controllable mesoporosity and enhanced catalytic properties.* RSC Advances, 2016. **6**(101): p. 99129-99138.

[54]   Benke, J.N.-S.M., *Micro-reactors: A new concept for chemical synthesis and technological feasibility.* Materials Science and Engineering, 2014. **39**(2): p. 89-101.

[55]   Robertson, K., *Using flow technologies to direct the synthesis and assembly of materials in solution.* Chemistry Central Journal, 2017. **11**(1): p. 4.

[56]   Bunaciu, A.A., E.G. UdriŞTioiu, and H.Y. Aboul-Enein, *X-ray diffraction: instrumentation and applications.* Critical reviews in analytical chemistry, 2015. **45**(4): p. 289-299.

[57]   Lenthe, W.C., et al., *Advanced detector signal acquisition and electron beam scanning for high resolution SEM imaging.* Ultramicroscopy, 2018. **195**: p. 93-100.

[58]   Suga, M., et al., *Recent progress in scanning electron microscopy for the characterization of fine structural details of nano materials.* Progress in Solid State Chemistry, 2014. **42**(1-2): p. 1-21.

[59]   Maraghechi, S., et al., *Correction of scan line shift artifacts in scanning electron microscopy: An extended digital image correlation framework.* Ultramicroscopy, 2018. **187**: p. 144-163.

[60]   Gerwert, K. and C. Kötting, *Fourier transform infrared (FTIR) spectroscopy.* Encyclopedia of Life Sciences, 2010.

[61]   Berthomieu, C. and R. Hienerwadel, *Fourier transform infrared (FTIR) spectroscopy.* Photosynthesis research, 2009. **101**(2-3): p. 157-170.

[62]   Liu, J., et al., *Determination of ash content and concomitant acquisition of cell compositions in microalgae via thermogravimetric (TG) analysis.* Algal Research, 2015. **12**: p. 149-155.

[63]   Gaisford, S., V. Kett, and P. Haines, *Principles of thermal analysis and calorimetry.* 2016: Royal society of chemistry.

[64]   Subbalakshmi, P. and N. Veeraiah, *Study of CaO–WO3–P2O5 glass system by dielectric properties, IR spectra and differential thermal analysis.* Journal of non-crystalline solids, 2002. **298**(1): p. 89-98.

[65]   Hussain, S.Z. and K. Maqbool, *GC-MS: Principle, Technique and its application in Food Science.* International Journal of Current Science, 2014. **13**: p. 116-126.

[66]   Mandal, S.C., V. Mandal, and A.K. Das, *Essentials of botanical extraction: principles and applications.* 2015: Academic Press.

[67]   Kumar, D., et al., *Bio-oil and biodiesel as biofuels derived from microalgal oil and their characterization by using instrumental techniques*, in *Algae and Environmental Sustainability*. 2015, Springer. p. 87-95.

[68]   Rakić, V. and L. Damjanović, *Temperature-Programmed Desorption (TPD) Methods*, in *Calorimetry and Thermal Methods in Catalysis*. 2013, Springer. p. 131-174.

[69]   Poulsen, H., et al., *Amorphous silica studied by high energy X-ray diffraction.* Journal of Non-Crystalline Solids, 1995. **188**(1-2): p. 63-74.

[70]   Rida, M.A. and F. Harb, *Synthesis and characterization of amorphous silica nanoparitcles from aqueous silicates uisng cationic surfactants.* Journal of Metals, Materials and Minerals, 2014. **24**(1).

[71]   Treacy, M.M. and J.B. Higgins, *Collection of simulated XRD powder patterns for zeolites fifth (5th) revised edition*. 2007: Elsevier.

[72]   Rutkowska, M., et al., *Hierarchically structured ZSM-5 obtained by optimized mesotemplate-free method as active catalyst for methanol to DME conversion.* Catalysis Science & Technology, 2016. **6**(13): p. 4849-4862.

[73]   Wu, W. and E. Weitz, *Modification of acid sites in ZSM-5 by ion-exchange: An in-situ FTIR study.* Applied Surface Science, 2014. **316**: p. 405-415.

[74]   Luo, J., et al., *Facile synthesis of monodispersed Au nanoparticles-coated on Stöber silica.* Colloids and Surfaces A: Physicochemical and Engineering Aspects, 2013. **425**: p. 83-91.

[75]   Wang, Y. and F. Caruso, *Mesoporous silica spheres as supports for enzyme immobilization and encapsulation.* Chemistry of Materials, 2005. **17**(5): p. 953-961.

[76]   Carcouet, C. and C. Camille, *Chemistry and morphology of silica nanoparticles*. 2014, Technische Universiteit Eindhoven.

[77]   Zhang, S., et al., *Size control of monodisperse silica particles by modified Stöber method.* Integrated Ferroelectrics, 2017. **178**(1): p. 52-57.

[78]   Silva, B., et al., *Evaluation of ion exchange-modified Y and ZSM5 zeolites in Cr (VI) biosorption and catalytic oxidation of ethyl acetate.* Applied Catalysis B: Environmental, 2012. **117**: p. 406-413.

[79]   Sanhueza, V., et al., *Synthesis of ZSM-5 from diatomite: a case of zeolite synthesis from a natural material.* Journal of Chemical Technology & Biotechnology: International Research in Process, Environmental & Clean Technology, 2004. **79**(7): p. 686-690.

[80]   Shaikh, I.R., et al., *H-ZSM-5 zeolite synthesis by sourcing silica from the wheat husk Ash: characterization and application as a versatile heterogeneous catalyst in organic transformations including some multicomponent reactions.* Journal of Catalysts, 2015. **2015**.

[81]   Ji, Y., H. Yang, and W. Yan, *Strategies to enhance the catalytic performance of ZSM-5 zeolite in hydrocarbon cracking: A review.* Catalysts, 2017. **7**(12): p. 367.

[82]   Zhang, S., et al., *Study on the synthesis of MFI and FER in the presence of n-butylamine and the property of n-butylamine in a confined region of zeolites.* RSC Advances, 2016. **6**(115): p. 114808-114817.

[83]   Jiang, S., et al., *Stability and deactivation of Fe-ZSM-5 zeolite catalyst for catalytic wet peroxide oxidation of phenol in a membrane reactor.* RSC Advances, 2015. **5**(51): p. 41269-41277.

[84]   Celik, A.G., A.M. Kilic, and G.O. Cakal, *Expanded perlite aggregate characterization for use as a lightweight construction raw material.* Physicochemical Problems of Mineral Processing, 2013. **49**.

[85]   JENTYS, A., G. RUMPLMAYR, and J. LERCHER, *Hydroxyl groups in phosphorus-modified HZSM-5.* Applied catalysis, 1989. **53**(2-3): p. 299-312.

[86]   Kubo, K., et al., *Comparison of steaming stability of Cu-ZSM-5 with those of Ag-ZSM-5, P/H-ZSM-5, and H-ZSM-5 zeolites as naphtha cracking catalysts to produce light olefin at high temperatures.* Applied Catalysis A: General, 2015. **489**: p. 272-279.

[87]   Konno, H., et al., *Kinetics of n-hexane cracking over ZSM-5 zeolites–effect of crystal size on effectiveness factor and catalyst lifetime.* Chemical engineering journal, 2012. **207**: p. 490-496.

[88]   Santilli, D.S., *Mechanism of hexane cracking in ZSM-5.* Applied Catalysis, 1990. **60**(1): p. 137-141.

[89]   Jolly, S., et al., *Reaction mechanisms and kinetics in the n-hexane cracking over zeolites.* Applied catalysis A: general, 1997. **156**(1): p. 71-96.

[90]   Kubo, K., et al., *Effect of steaming on acidity and catalytic performance of H-ZSM-5 and P/H-ZSM-5 as naphtha to olefin catalysts.* Microporous and Mesoporous Materials, 2014. **188**: p. 23-29.

[91]   Corma, A., J. Mengual, and P.J. Miguel, *IM-5 zeolite for steam catalytic cracking of naphtha to produce propene and ethene. An alternative to ZSM-5 zeolite.* Applied Catalysis A: General, 2013. **460**: p. 106-115.

[92]   Ji, Y., H. Yang, and W. Yan, *Catalytic cracking of n-hexane to light alkene over ZSM-5 zeolite: Influence of hierarchical porosity and acid property.* Molecular Catalysis, 2018. **448**: p. 91-99.